Improved Precision and Reference Materials for Stable Carbon Isotope Analysis in Basaltic Glasses using Secondary Ion Mass Spectrometry

Joshua Shea, Ery Hughes, Robert Balzer, Ilya Bindeman, Jon Blundy, Richard Brooker, Roman Botcharnikov, Pierre Cartigny, EIMF, Glenn Gaetani, Geoff Kilgour, John Maclennan, Brian Monteleone, David A. Neave, Oliver Shorttle

Author affiliations and correspondence details are on the following page.

This is a preprint of a manuscript submitted to **GEOSTANDARDS AND GEOANALYTICAL RESEARCH.**

Improved Precision and Reference Materials for Stable Carbon Isotope Analysis in Basaltic Glasses using Secondary Ion Mass Spectrometry

Joshua Shea[1,#,*], Ery Hughes[2,3,#,*], Robert Balzer[4], Ilya Bindeman[5], Jon Blundy[6], Richard Brooker[3], Roman Botcharnikov[7], Pierre Cartigny[8], EIMF[9], Glenn Gaetani[10], Geoff Kilgour[2], John Maclennan[1], Brian Monteleone[10], David A. Neave[4,11], Oliver Shorttle[1,12,*]

[1]Department of Earth Sciences, University of Cambridge, Cambridge, CB2 3EQ, United Kingdom

[2]GNS Science Te Pū Ao, 1 Fairway Drive, Lower Hutt, 5040, Aotearoa New Zealand

[3]School of Earth Sciences, University of Bristol, Wills Memorial Building, Queens Road, Bristol BS8 1RJ, United Kingdom

[4]Leibniz Universität Hannover, Institut für Mineralogie, Callinstrasse 3, 30167 Hannover, Germany

[5]Department of Earth Sciences, University of Oregon, Eugene, Oregon, 97403, United States of America

[6]Department of Earth Sciences, University of Oxford, South Parks Road, Oxford, OX1 3AN, United Kingdom

[7]Institut für Geowissenschaften, Johannes Gutenberg Universtät Mainz, J.-J.-Becher-Weg 21, Mainz, 55128, Germany

[8]Université de Paris Cité, Institut de Physique du Globe de Paris, F-75005, Paris, France

[9]Edinburgh Ion Microprobe Facility, University of Edinburgh, Edinburgh, UK

[10]Department of Geology and Geophysics, Woods Hole Oceanographic Institution, Woods Hole, MA, 02543, United States of America

[11]Department of Earth and Environmental Sciences, The University of Manchester, Manchester, Oxford Road, M13 9PL, United Kingdom

[12]Institue of Astronomy, University of Cambridge, Cambridge, CB3 0HA, United Kingdom

[#]Authors contributed equally

[*] Corresponding authors: JS jjs83@cam.ac.uk; EH e.hughes@gns.cri.nz; OS os258@cam.ac.uk

Abstract

We introduce three new reference materials and a new high-precision set-up for stable carbon isotope analysis in basaltic glasses using large-geometry secondary ion mass spectrometry (SIMS) instrument. The new hydrous basaltic reference materials,

characterised for carbon concentration and isotope composition by step-heating gas extraction and manometry followed by isotope ratio mass spectrometry, show homogeneity for *in situ* analysis. Additionally, their hydrogen concentration and hydrogen isotope ratios are reported. Our SIMS protocol uses multi-collection, cycling between concurrent measurements of ^{12}C and ^{13}C on electron multipliers, and either ^{30}Si or ^{18}O, as a reference mass, on a 10^{11} Ω resistor Faraday cup. The analysis involves rastering over an area of 20 μm^2 for 100 cycles, resulting in a 40 μm-wide analytical pit. This set-up achieves high internal precision for $\delta^{13}C$ down to $\pm$ 0.35 ‰ 1RSE at 1706^{+89}_{-88} $\mu g\ g^{-1}$ CO_2, with precision of $\pm$ 1.00 ‰ 1RSE or better between $163^{+5.1}_{-5.2}$ and $267^{+8.9}_{-8.9}$ $\mu g\ g^{-1}$ CO_2, depending on set-up sensitivity. Precision reported here is improved by a factor of three at comparable concentrations to that previously reported elsewhere. Carbon blanks were characterised by measuring carbon-free olivines, allowing for accurate blank corrections on $\delta^{13}C$ measurements. After correcting for blank signals and instrument mass fractionation, we measure $\delta^{13}C$ in glasses with low CO_2 concentrations down to $26.16^{+0.85}_{-0.86}$ $\mu g\ g^{-1}$ CO_2 with a final measurement standard sample deviation of $\pm$ 2.97 ‰ 1s. We report *in situ* measurements on an ocean floor basaltic glass from the East Pacific Rise and a set of synthetic basaltic glasses are presented to demonstrate our approach. The reference materials and SIMS set-up can be used to significantly improve the accuracy and precision of del13C measurements in natural basaltic glasses and are applicable across a wide range of geologically relevant carbon contents.

Keywords: Carbon; Carbon Isotopes; low concentration; secondary ion mass spectrometry; basalt; glass.

1 Introduction

Carbon is a volatile, atmophile, element with two stable isotopes ^{12}C and ^{13}C, that have natural abundances of 99% and 1%, respectively (Meija et al., 2016). In common mid-ocean ridge and ocean-island basalts carbon is oxidised and therefore has low solubility and therefore is present in low concentrations (Jendrzejewski et al., 1997). Typically, carbon, as CO_2, is typically the first volatile to exsolve from basaltic melts, and depending on the degassing mechanism and fraction exsolved, degassing can dramatically alter the carbon isotope ratio of the melt, potentially by tens of per mil (Figure 1; e.g., Aubaud, 2022; Macpherson and Mattey, 1994; Pineau and Javoy, 1994). This fractionation can occur at equilibrium or through kinetic processes, and during either closed- or open-system degassing mechanisms, all leading to substantial modification of the gas- and melt-phase carbon isotope ratios away from the system's initial bulk composition (Figure 1; e.g., Aubaud, 2022). Being able to differentiate between these degassing mechanisms can elucidate how carbon is released from basaltic melts, allowing for improved modelling linking volcanism and climate, reconstructions of primary carbon concentrations in primitive melts, and the characterisation of mantle carbon reservoirs.

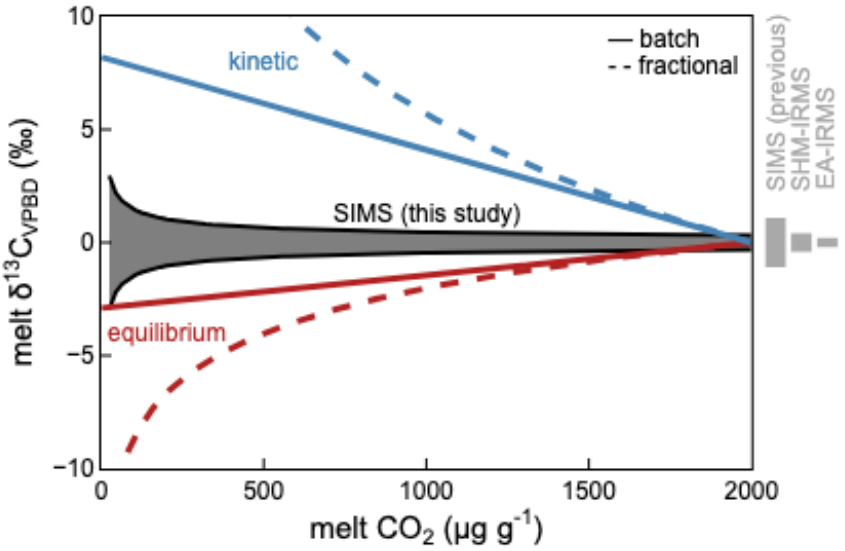

Figure 1 Carbon isotopic composition of a basaltic melt during progressive degassing from an initial CO_2 = 1000 µg g^{-1} and $\delta^{13}C = 0$ ‰ under different regimes: fractional (dashed curves) or batch (solid curves) and equilibrium (red: fractionation factor = $+2.9$ ‰ (Lee et al., 2024) or kinetic (blue: -8.2 ‰ (Javoy and Pineau, 1991). Uncertainty (1s) for different techniques is shown, either as shaded regions around 0 ‰ $\delta^{13}C$ for SIMS from this study or bars outside the panel for previous SIMS protocols (Lee et al., 2024) compared to bulk techniques such as SHM-IRMS (e.g., Macpherson et al., 1999) and EA-IRMS; (e.g., Lee et al., 2024).

Improved precision at high spatial resolution is key for answering science questions at the micron scale relating to carbon degassing and the preservation of primary carbon isotope ratios in magmatic systems. As carbon degasses early and extensively from melts, to achieve these insights it often requires seeing back earlier into the history of degassing magmas (Blundy and Cashman, 2008), before they have lost significant amounts of carbon (Aubaud, 2022). The most effective way to do this is often by analysing mineral-hosted melt inclusions, small pockets of melt trapped inside growing crystals at depth in the magmatic system. Accessing this archive of early carbon degassing requires *in situ* techniques capable of high spatial resolution and analytical

precision, as suitable melt inclusions will often be less than $100\ \mu m$ across (Blundy and Cashman, 2008).

2 Background

Pioneering work by Hauri (2002) first demonstrated measurements of carbon isotope ratios by SIMS on natural silicate glasses. For standards a natural basaltic glass from the East Pacific Rise, ALV981-R23, which contained $405.7 \pm 8.0\ \mu g\ g^{-1}\ CO_2$ was used (Des Marais, 1986; Fine and Stolper, 1986, 1985; Macpherson et al., 1999; Pineau and Javoy, 1983), along with a synthetic basaltic glass, SAV-C-1, which contained 7000 $\mu g\ g^{-1}$ of CO_2. Measurements on three melt inclusions were reported, however the low precision of the reported measurements, an unusual fractionation trend, and lack of reference materials delayed wider uptake of the SIMS method to analyse carbon isotope ratios in volcanic glasses. Later, Le Voyer et al. (2014), in a conference abstract, reported SIMS analytical error of $\pm 2 - 3\ ‰$ reproducibility on low carbon glass reference materials ($100 - 400\ \mu g\ g^{-1}\ CO_2$). Lee et al. (2024) presented a SIMS set-up along with 31 synthetic basaltic glass reference materials, synthesised using a piston cylinder apparatus. Their reference materials were externally measured for carbon isotope ratios by a single-step pyrolysis Elemental Analyser (EA)-IRMS technique, and the CO_2 concentration was measured by Fourier Transform Infrared (FTIR) spectroscopy, ranging $380 - 12000\ \mu g\ g^{-1}$. Their reported precision was $\pm 1.1\ ‰$ (1s, reported as the averaged internal and external precision) at CO_2 concentrations down to $1800\ \mu g\ g^{-1}$. At the time of writing these new reference materials have not been used to characterise natural glasses.

There are challenges when conducting *in situ* carbon isotope measurements, particularly at low carbon concentrations $< 125\ \mu g\ g^{-1}\ CO_2$ at mid ocean ridges (Jendrzejewski et al., 1997) or after significant degassing has occurred, where isotopic fractionation is most extreme (Figure 1: Hauri, 2002; Hauri et al., 2002; Le Voyer et al., 2014; Lee et al., 2024). Carbon isotope measurements are routinely analysed in basaltic glasses by bulk analysis, via stepped-heating extraction and manometry combined with isotope ratio mass spectrometry (SHM-IRMS; e.g., Macpherson et al., 1999). This bulk technique enables the separation of surface and/or adsorbed carbon contamination, the carbon trapped in vesicles, and the dissolved carbon inventory by sequentially heating the sample to higher temperatures, typically releasing the dissolved magmatic carbon between 900 and $1300°C$ (e.g., Aubaud, 2022; Des Marais, 1986; Exley et al., 1986; Mattey et al., 1989, 1984; Swart et al., 1983). Raman spectroscopy has been used to analyse *in situ* carbon isotope ratios in silicate melts (Mysen, 2017, 2016), but typically the carbon concentration is too low in silicate glasses to observe the carbonate ion peak (Morizet et al., 2013). Raman hot bands have been used to analyse carbon isotope ratios of CO_2 vapor in fluid inclusions, but this is difficult since this method requires high carbon density (Wang et al., 2024; Wang and Lu, 2023). Therefore, *in situ* measurements of the dissolved magmatic component in volcanic glasses have mostly focused on improving large geometry Secondary Ion Mass Spectrometry (SIMS) techniques capable of maintaining high transmission at high spatial resolution (Fitzsimons et al., 1999; Hauri et al., 2002).

The precision of carbon isotope ratios in basaltic glasses measured by SIMS is restricted, particularly in basaltic melts with at low carbon concentrations, by counting statistics, a low ^{13}C natural abundance, and carbon contamination. Carbon

concentrations in mid ocean ridge glasses reach saturation between $125-250\ \mu g\ g^{-1}\ CO_2$ (Jendrzejewski et al., 1997), whereas melt inclusions trapped at great depth, like those El Herrio, Canary Islands at trapped at 7.5 kbar, contain up to $3600\ \mu g\ g^{-1}\ CO_2$ (Taracsák et al., 2019). For applications across all CO_2 concentrations, high sensitivity measurements of ^{13}C, are required, since its abundance of 1% limits precise determinations (Fitzsimons et al., 1999; Meija et al., 2016). Transmission of ^{13}C can be further limited by a large polyatomic interference of $^{1}H^{12}C$ on ^{13}C, which requires a mass resolving power of > 4300 to deconvolute (Fitzsimons et al., 1999). Achieving that mass resolution comes with the expense of transmission, and therefore requires a large geometry SIMS to maintain adequate transmission (Fitzsimons et al., 1999; Wang et al., 2018). Carbon contamination inherent to SIMS analyses is driven by carbon present in the vacuum of analytical equipment from organic vacuum pump lubricants, and surface contamination driven by adsorption onto the glass surface (Keppler et al., 2003). Collectively, these extrinsic carbon sources are termed the *'blank'* (Hauri et al., 2002, 2002; Le Voyer et al., 2014; Lee et al., 2024). The effect of the blank on isotope ratio determinations can be especially prominent where there is a large isotope ratio difference between the sample and blank. A SIMS set-up focused on obtaining high-precision carbon isotope ratio measurements therefore requires enhanced transmission, resolved interferences, and a low, measurable carbon blank. Under these circumstances the precision of an *in situ* SIMS measurement may approach that of bulk analyses, usually at the expense of long analysis times (Fitzsimons et al., 2000).

For SIMS measurements to also return precise and accurate absolute carbon isotope ratio and concentrations measurements matrix-matched standard materials are

required. These materials need to have known carbon concentrations and isotope ratios (e.g., Blundy and Cashman, 2008; Lockyer et al., 2024). A popular approach is to synthesise reference materials using a high-pressure apparatus; however, care must be taken to avoid heterogeneity, which may not be recognised in external bulk determinations. Additional issues for carbon isotope ratios may arise; the common use of graphite furnaces in piston cylinder assemblies, for example, can result in ^{12}C diffusion through metal capsules that are otherwise employed to contain volatiles within an experimental charge (Brooker et al., 1998). ^{12}C diffusion can produce sample heterogeneity from isotopic ratio gradients across an experimental charge, and ratios that deviate significantly from natural magmatic materials (Brooker et al., 1998). Heterogeneity of a reference material can affect the calculation of the Instrument Mass Fractionation (IMF) factor ($\alpha = \frac{^{13}C/^{12}C_{measured}}{^{13}C/^{12}C_{known}}$), which can propagate through to the final isotope delta calculation when α is applied to the isotope ratio measurement.

We introduce three new reference materials, ETNA24, ETNA32, and ETNA36, and an improved set-up for high-precision measurements of stable carbon isotope ratios in basaltic glasses using large geometry-SIMS. To characterise the magmatic carbon component and exclude surface contamination from the bulk determination, we used SHM-IRMS. Our reference materials were additionally characterised for hydrogen concentration and isotope ratios using a thermal conversion elemental analyser combined with IRMS (TCEA-IRMS). Carbon and hydrogen concentrations were also analysed using FTIR, SIMS, and Raman microanalytical techniques. The application of the new reference materials combined with improved SIMS precision are demonstrated on synthetic basaltic glasses and an ocean floor basaltic glass from the East Pacific Rise.

We focused on a SIMS set up that minimises blank carbon contamination and enhances sample transmission at concentrations relevant for natural systems in order to precisely determine magmatic carbon isotope ratios. We also demonstrate the role of blanks with low carbon isotope ratios and discuss how these can influence the true sample isotope ratio. Our approach achieves high internal precision, of ± 0.35 ‰ 1RSE at 1706^{+89}_{-88} $\mu g\, g^{-1}$ CO_2, and a precision exceeding ± 1.00 ‰ 1RSE between $163^{+5.1}_{-5.2}$ and $267^{+8.9}_{-8.9}$ $\mu g\, g^{-1}$ CO_2, with the final precision of the measurement comparable to current bulk measurements.

3 Materials and Methods

3.1 Synthesis and Characterisation of Reference Materials

3.1.1 Experimental synthesis

Experimental glasses were synthesised using two different starting compositions (A: ETNA24, and B: ETNA32 and ETNA36). Experimental synthesis of ETNA24 was described in the Supplementary Material of Hughes et al. (2018). Albite, anorthite, sanidine, fayalite, wollastonite, SiO_2, MnO, MgO, TiO_2, Fe_2O_3, and $Ca_3(PO_4)_2$ powders were mechanically mixed by grinding under water in an agate mortar and dried under a heat lamp for 30 $mins$. B glasses were glassed at 1 atm in air in a Pt-crucible at 1300°C for one hour in the GERO™ vertical furnace at the School of Earth Sciences, University of Bristol, UK. To avoid oxidation during glassing, fayalite and Fe_2O_3 were added after this step for B glasses.

The volatile-free starting mixture was dried overnight (~ 100°C) before $CaCO_3$ was added. To give variable carbon compositions, $CaCO_3$ was added as either powdered

Seaford Head Chalk (SHC) with organic matter removed using the method of Barker et al. (2003) to give a relatively high carbon isotope ratio (Jenkyns et al., 1994); Oka carbonatite calcite (OKA) for lower isotope ratios (Deines, 1970); or a 50:50 mechanical mixture of the two (MIX). The carbonated starting mixture was dried overnight ($\sim 100°C$) before H_2O was added to the experimental capsule using a microsyringe. Starting compositions are detailed in Supplementary Material.

Large capsules, 5 mm in diameter and $15-30$ mm in length made of $Au_{75}Pd_{25}$, were loaded with $300-500$ mg starting powders plus H_2O produce sufficient material for bulk analysis and welded shut at each end. Capsules were immersed in water at $\sim 50°C$ then put in a $\sim 100°C$ oven for ~ 10 mins to check for leaks. Experiments were run in an internally heated pressure vessel (IHPV) at $1250°C$ and 3 (ETNA36), 5 (ETNA24), or 7 (ETNA32) kbar using Ar gas as the pressurising medium at the Institut für Mineralogie, Leibniz Universität Hannover, Germany. The IHPV was chosen to avoid carbon infiltration from the graphite furnace in a piston cylinder apparatus that can result in heterogenous $\delta^{13}C$ in experimental glasses (Brooker et al., 1998; King et al., 2002). Experiments were run for $\sim 18-36$ hours. The sample holder was equipped with four S-type thermocouples: two were used to control the furnace temperature and two were used to record the sample temperature. Temperature varied by $< 5°C$ during experiments. Samples were quenched at the end of runs by fusing the Pt wire on which they were suspended in the IHPV, resulting in cooling rates of $\sim 150°C\ s^{-1}$ (Berndt et al., 2002).

Sample capsules did not gain or lose weight outside weighing uncertainties during experimental runs and had convex shapes confirming that they remained volatile undersaturated. Capsules were opened under a binocular microscope and glass chips

were selected for further analysis. All run products were dark brown and glassy, with no evidence for crystals, microlites, or internal vesicles. No magnetite nanolites were detected using Raman spectroscopy (Supplementary Figure S3).

3.1.2 Glass composition using EPMA

Glass compositions were analysed using EPMA on the JEOL JXA 8530F Hyperprobe at the School of Earth Sciences, University of Bristol, UK. The analytical protocol for ETNA24 is described in the Supplementary Material of Hughes et al. (2018). For ETNA32 and ETNA36, analyses used a $15\,\mathrm{kV}$ accelerating voltage, $10\,\mathrm{nA}$ beam current, and $5-10\,\mu\mathrm{m}$ beam size. Elements measured, spectrometer set-up, on-peak count times, and primary standards for peaking-up and calibration are detailed in Supplementary Material. Mean atomic number backgrounds were used instead of collecting counts off-peak (Donovan and Tingle, 1996). Time-dependent intensity data were collected for Ca, Si, Na, K, and Fe in case of element migration (Nielsen and Sigurdsson, 1981). At least ten analyses on fresh areas of glass were averaged per experimental glass. For all glasses, quantification used the Probe for EPMA software and water was included as an element by difference. Individual analyses and secondary standard data are provided in Supplementary Material.

3.1.3 Bulk carbon concentration and isotope ratio by SHM-IRMS

Step-heating extraction of carbon-bearing species was performed using a vacuum line at the Laboratoire de Geochimie des Isotopes Stables, Institut de Physique du Globe de Paris, France (e.g., (Pineau et al., 1976; Pineau and Javoy, 1994). Glasses were crushed then sieved, and chips between $240-460\,\mu\mathrm{m}$ were used for subsequent analysis. Prior to analysis, glass chips were washed in a 50:50 mixture of dichloro-

methane and -methanol in an ultrasonic bath before being dried in an oven at $\sim 100°C$ overnight.

Glass chips were weighed and then transferred into a ball-and-cup holder suspended within the vacuum line. The concentration and isotope ratio of carbon present in the vacuum line (the 'blank') was quantified to correct sample measurements. The protocol for running blanks and sample was the same. The Pt-crucible was heated via induction to a given temperature for $30\ \mathrm{mins}$. Any volatiles released were oxidised by a CuO furnace heated to $850°C$ and condensable gases (e.g., CO_2 and H_2O) were collected in a liquid N_2 trap at $-190°C$. The Pt-crucible and CuO furnace $(250°C)$ were cooled for $30\ \mathrm{mins}$, absorbing any remaining free oxygen. Any non-condensable gases present were removed, drawing any remaining CO_2 into the liquid N_2 trap. The liquid N_2 trap was heated to $-140°C$, releasing CO_2 that was collected in a separate liquid N_2 trap. This was heated to room temperature and then measured using a calibrated barometer.

After a new sample was introduced into the vacuum line, blank analyses were conducted at $1400 - 1450°C$ until the carbon concentration was typically $\leq 0.1\ \mu\mathrm{mol\ C}$. The carbon released during the final blank, before the actual glass was analysed, was normally collected to quantify its carbon isotope ratio. The sample was introduced into the Pt-crucible by lowering the ball-and-cup holder, which meant the vacuum was not broken between blank and glass analysis. The glass was heated incrementally to increasing temperatures to release the volatiles in stages. The exact temperature steps chosen to release carbon varied between glasses. Typically, the glass was heated in steps of $50 - 100°C$ from $\sim 500°C$ until a near blank value was reached, which indicated all the low temperature, adsorbed CO_2 had been released (e.g., Mattey et al., 1984). After this,

the sample was heated in a single step to $\sim 1200°C$ to release all dissolved carbon and minimise the influence of the blank. The sample was further heated in $\sim 100°C$ steps to $\sim 1400°C$ to ensure all carbon had been released, including repeats of temperature steps if necessary.

The carbon isotope ratio of the gas extracted at each temperature step and the blanks were measured using IRMS on the Thermo DELTA plus XP IRMS equipped with a mirco-volume device at the Laboratoire de Geochimie des Isotopes Stables, Institut de Physique du Globe de Paris, France (e.g., Aubaud, 2022). Samples containing only a few μmoles of CO_2 were cooled in liquid N_2 to increase their flow rate if required to improve analysis.

3.1.4 Bulk water and hydrogen isotope ratio by TCEA-IRMS

Measurements of water concentration and δD_{SMOW} (where $\delta D_{SMOW} = \left(\left(\frac{^2H/^1H_{Sample}}{^2H/^1H_{SMOW}}\right) - 1\right)$, expressed in per mill, ‰, and VSMOW is the Vienna Standard Mean Ocean Water, VSMOW value of $^2H/^1H$ value of 0.015576, IAEA) were made at the Department of Earth Sciences, University of Oregon, USA, using the method of Nolan and Bindeman (2013). Glass chips were crushed to $50 - 150$ μm to aid melting, weighed to a precision of 1 μg, and folded into silver foil capsules for analysis. H_2O was extracted using TCEA at $1450°C$ using glassy carbon. The thermally released H_2O was transformed into H_2 and CO gases and these were separated by gas chromatography in a He flow and then transferred for concentration and isotope measurement to a large radius MAT253 10 kV gas source IRMS in a continuous flow mode. Calibration used biotite and muscovite mineral standards with $3.5 - 4.03$ % g g^{-1} H_2O and -91.5 to -28.4 ‰ δD (NBS30: Gonfiantini, 1984; USGS57 and USGS58: Qi et al., 2017, and BUD biotite at -151 ‰). δD

values were derived by a linear 3 point correlation of the standard covering the δD of the unknowns. The average accuracy (1s) of reference materials run during the analysis were ± 0.06 % g g^{-1} H_2O and ± 0.9 ‰ δD, see Hudak et al. (2022) for further details.

3.2 SIMS Analytical Set-up for $\delta^{13}C$

Care was taken when handling samples to avoid carbon adsorption onto surfaces to minimise the carbon background signal during analysis. Reference glass fragments and either an olivine from a lava flow in Miðfell, Iceland ($Fo_{\sim 90}$) or a San Carlos Olivine were polished to $\sim 1\ \mu m$ mirror finish and embedded into indium mounts. Indium was used as a mounting medium to avoid carbon contamination and to minimise background carbon signals from outgassing of organic carbon from epoxy resin under vacuum (Hauri, 2002). Olivines were co-mounted with the glasses to monitor the carbon blank in the measurements, since carbon solubility in olivine is exceedingly low (~ 0.1 µg g^{-1}, Keppler et al., 2003). Mounts were thoroughly cleaned using deionised water and dried in an oven at $60–70°C$ for at least 1 hour. After cleaning, mounts were gold coated to provide a conductive surface.

Preliminary carbon isotope analyses were carried out at the Edinburgh Ion Microprobe Facility, UK, as described in Hughes (2019) on a Cameca IMS-1270 at the Edinburgh Ion Microprobe Facility at The University of Edinburgh. Subsequent method development was carried out on a Cameca IMS-1280 at the Northeast National Ion Microprobe Facility at Woods Hole Oceanographic Institute (WHOI), USA. Measurements at WHOI were conducted over two sessions in February and July 2024. Prior to analysis, glasses were degassed in a primary airlock for a minimum of 1 hour but were typically

under vacuum overnight. Analyses were conducted in the secondary analytical chamber at pressures ranging between 2×10^8 and 6×10^{10} torr, with analyses typically run at 3.3×10^9 torr. A $^{133}Cs^+$ primary beam was used, and we applied an acceleration voltage of 10 kV to produce a beam current of 10 nA at the sample surface. This produced a negative charged secondary ion beam with an acceleration voltage of 10 kV. An electron flood gun at the sample surface was used to avoid charging. The primary ion beam was rastered over a 25 x 25 μm^2 area for 300 s. After pre-sputtering, the secondary ion beam was centred with respect to the entrance slit and field aperture, and an energy slit adjustment was made. During the analysis the beam raster was reduced to 20 x 20 μm^2, which was used to minimise the blank by mitigating surface carbon entering the pit during analysis, with this resulting in a 40 μm analytical pit width within the larger 50 μm width pre-sputter pit.

We used multicollection to count negatively charged secondary ions, adjusting the B-field of the secondary magnet to centre the axial mass and to separately count carbon masses and either the ^{30}Si or ^{18}O reference masses. We concurrently counted ^{12}C and ^{13}C on separate electron multiplier detectors on trolley positions L2 and H2, centred on mass 12.5, with a deadtime of 63.1 and 63.7 ns. After pre-sputtering and prior to the analysis, a high voltage adjustment was performed on position L2 to mitigate aging effects from high ^{12}C counts. Either ^{30}Si or ^{18}O was measured on a 10^{11} Ω resistor Faraday cup detector at trolley position H1, centred at masses 29.9 or 17.9. The analysis was performed over 100 cycles, where each cycle consisted of 12 second count times for ^{12}C and ^{13}C, while ^{30}Si or ^{18}O were collected for 2 seconds, with wait times of 3 seconds for ^{12}C and ^{13}C and 2 seconds for ^{30}Si of ^{18}O. To avoid internal drift introduced from cycling

between masses 12.5 and either 29.9 or 17.9 throughout the analysis, a mass calibration adjustment was performed automatically prior to the analysis and at 25 cycle intervals. Overall, including the pre-sputtering, this routine resulted in a 43-minute total analysis time.

Parameters for the secondary ion beam were set-up to reduce blank signal while maintaining reasonable transmission for precise measurements of ^{13}C. We applied a contrast aperture with a diameter of $400\ \mu m$, an entrance slit of $122\ \mu m$, and an energy slit of $50\ \mu m$. Analyses were conducted using a field aperture of $2500\ \mu m^2$ to block transmission of secondary ions from outside of the centre-most $31.25\ \mu m^2$ of the sample crater. For glasses with high carbon concentration, we reduced the field aperture size to achieve a maximum of $\sim 500{,}000$ counts per second of ^{12}C on the ETNA24 reference material. We chose this to minimise surface contribution to the total measurement signal and mitigate degradation of the electron multiplier detector. A $250\ \mu m$ slit was placed in front of each detector, which achieved a mass resolving power of ~ 5000, sufficient to resolve the $^{1}H^{12}C$ polyatomic interference on ^{13}C.

Stable carbon isotope ratios are reported relative to the Vienna Pee Dee Belemnite (VPDB) primary reference material (Brand et al., 2014), as;

$$\delta^{13}C_{VPDB} = \left(\left(\frac{^{13}R_{Sample}}{^{13}R_{VPDB}}\right) - 1\right), \quad (1)$$

where $^{13}R_{Sample}$ and $^{13}R_{VPDB}$ are respectively the $^{13}C/^{12}C$ ratio of the mean deadtime-corrected value of the sample after corrections for instrumental mass fractionation and the VPDB ratio ($^{13}R_{VPDB} = 0.011100$; Fitzsimons et al., 2000; Hoffman and Rasmussen,

2022). $\delta^{13}C_{VPDB}$ values (hereafter referred to as $\delta^{13}C$) are small and are reported in parts per thousand using per mil (‰) notation (Coplen, 2011).

Multiple reference masses, ^{30}Si, $^{28}Si^{2+}$ and ^{18}O. $^{28}Si^{2+}$ were tested, and both ^{30}Si and ^{18}O were used on separate runs to quantify CO_2 concentration. Carbon concentration was calibrated using background subtracted measurements on in-house reference materials at WHOI (519-4-1, 46D, D52-5, D51-3, D30-1: $0.11 - 1.59$ % g g^{-1} H_2O), combined with SHM measurements on ETNA24 and ETNA36.

4 Composition of Reference Materials

4.1 Blank correction for carbon concentration and isotope ratio

For any measurement, $\delta^{13}C$ is a weighted average of the sample and the blank, which can be approximated by the following equation when δ is small:

$$\delta_m n_m = n_s \delta_s + n_b \delta_b, \quad (2)$$

where n represents the quantity of carbon, and subscripts refer to the measured (m), sample (s) and the blank (b) (e.g., eq. (4) from Gelwicks and Hayes, 1990). Carbon blanks can significantly influence the $\delta^{13}C$ measurement, causing a deviation from the true $\delta^{13}C$ of a sample. This is pronounced in samples with low carbon concentrations and where large differences exist between the sample and blank $\delta^{13}C$; for example, a mantle carbon signature ($\delta^{13}C = -5$ ‰) mixing with an organic component ($\delta^{13}C = -25$ ‰). A blank-correction is therefore required for both SHM-IRMS and SIMS analyses of $\delta^{13}C$ and CO_2 concentration.

The blank-corrected $\delta^{13}C$ is calculated by re-arranging eq (2), where $n_s = n_m - n_b$, such that:

$$\delta_s = (n_m\delta_m - n_b\delta_b)/(n_m - n_b), \quad (3)$$

(e.g., eq. (10) from Gelwicks and Hayes, 1990). The error from the blank and measurement are propagated to the corrected sample $\delta^{13}C$ using:

$$\sigma^2_{\delta_s} = \left(\frac{1}{(n_m - n_b)^2}\right)\left[\left(\frac{(\delta_m - \delta_b)^2}{(n_m - n_b)^2}\right)\left(n_b^2\sigma^2_{n_m} + n_m^2\sigma^2_{n_b}\right) + n_m^2\sigma^2_{\delta_m} + n_b^2\sigma^2_{\delta_b}\right], \quad (4)$$

where σ is the standard deviation of the error on the value indicated by the subscript (e.g., eq (14) from Gelwicks and Hayes, 1990).

Carbon released at each temperature-step during SHM-IRMS is blank-corrected using eq. (3) and (4). The blank composition is either measured prior to the sample being analysed (note that the vacuum is not broken between the blank and the sample) or assumed based on the values of blanks measured throughout the analyses (further details in Supplementary Material), and ranges between -25 to -20 ‰ $\delta^{13}C$ at $0.09–0.34$ μmol C. The total dissolved carbon concentration in the glass is the sum of the blank-corrected moles of carbon for all temperature-steps associated with dissolved (i.e., non-adsorbed) carbon, divided by the sample weight (measured to 10 μg precision). The overall isotope ratio is calculated by summing the blank-corrected isotope ratios of dissolved carbon weighted by the blank-corrected moles of carbon in that temperature-step. The error on the overall isotope ratio is calculated using:

$$\sigma_{\overline{\delta_s}} \cong \sqrt{\sum_{j=1}^{n} \left(f_j \sigma_{\delta_s^j} \right)^2}, \quad (5)$$

where j represents the number of temperature-steps and f is the fraction of total dissolved carbon in each temperature-step that contains dissolved carbon (i.e., eq. (6) from Hemingway et al., 2017).

4.2 Composition and homogeneity of reference materials

Measured and blank-corrected carbon concentrations and isotope ratios are reported in the Supplementary Material and shown in Figure 2. All glasses show three stages of carbon release at $\sim 500 - 600$ (low), $\sim 600 - 1200$ (medium), and $\sim 1200 - 1400$ (high) °C, with low, high, and variable $\delta^{13}C$ signatures, respectively (Figure 2). The carbon released at low temperature ($< 600°C$) is attributed to a combination of surficial and adsorbed carbon and does not represent carbon dissolved within the glass (e.g., Des Marais, 1986; Exley et al., 1986; Macpherson et al., 1999; Mattey et al., 1984). Hence, the low-temperature carbon has a very low isotope ratio (< -20 ‰ $\delta^{13}C$; Macpherson et al., 1999; Mattey et al., 1984). We attribute the carbon released at medium to high temperatures as carbon dissolved in the glass. Previous studies observed dissolved carbon to be released at $> 900°C$ (e.g., Aubaud, 2022). However, as these experimental glasses are hydrous, the CO_2 is released at lower temperatures compared to previous results on anhydrous glass. The medium-to-high temperature carbon has higher isotope ratios than the low temperature contaminant as the $\delta^{13}C$ of the $CaCO_3$ added to the starting materials with isotopically higher $\delta^{13}C$ (-5 to +2 ‰). The experimental glasses

contained no internal vesicles: hence, there should be no release of CO_2 from vesicles at $800–1000°C$ (Mattey et al., 1984).

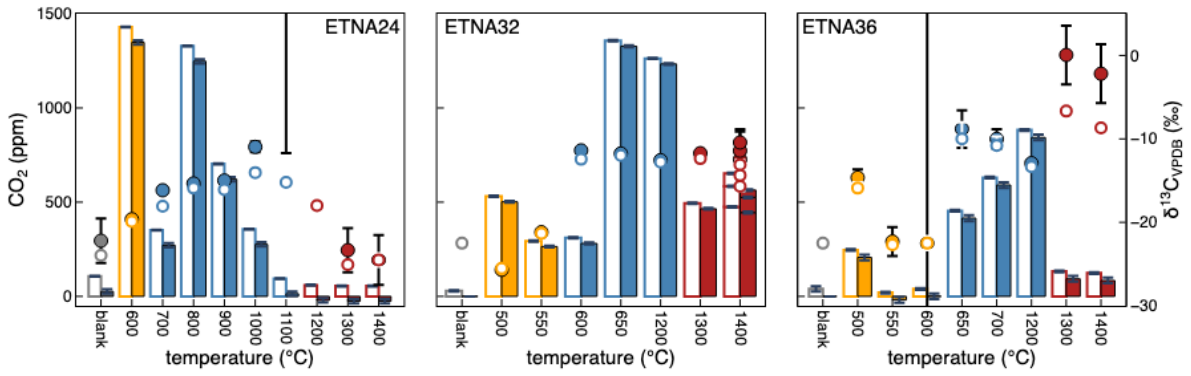

Figure 2 Results from step-heating extraction and manometry combined with isotope ratio mass spectrometry (SHM-IRMS). Bars indicate amount of carbon released (left axis) and points are the corresponding $\delta^{13}C$ (right axis) for the temperature step shown on the x-axis (temperatures are quoted to the nearest $100°C$). Measured values are shown using open symbols and blank-corrected values are filled-symbols, where the colour indicates the inferred type of carbon released (grey = blank, orange = surficial/adsorbed, blue = dissolved, and red = high-temperature). Error bars are smaller than the symbol if not visible.

A detailed discussion of the SHM-IRMS results of each sample is included in Supplementary Material to evaluate the reliability of the measurement and estimate its error. All glasses had good separation between adsorbed and dissolved carbon during SHM, critical for accurate quantification. ETNA24 had significant carbon adsorption, such that it was too high to be quantified by the capacitance manometer, but it represented at least 36% of the blank-corrected measured carbon. Therefore, at a minimum, the CO_2 concentration would have been 68% higher and the $\delta^{13}C$ would have been 2.2 ‰ lower than the true values were a single-step pyrolysis technique used (calculation details in Supplementary Material; Supplementary Figure S2). ETNA32 and ETNA36 contained less adsorbed carbon (17% and 9%, respectively, of blank-corrected

measured carbon) but would have had 39% and 12% higher CO_2 contents and 2.0 and 0.6 ‰ lower $\delta^{13}C$ with a single-step pyrolysis technique. We hypothesise that ETNA24 contained more adsorbed carbon because the time between opening the experimental capsule and SHM analysis was longer than for ETNA32 and ETNA36 (nine vs. five months). Adsorbed carbon becomes problematic with low sample CO_2 concentration and a large difference between the isotope ratio of the sample and adsorbed carbon (i.e., away from -25 to -20 ‰ $\delta^{13}C$). Adsorbed hydrogen is not thought to effect TCEA to the same extent and good agreement has been found between FTIR and step-heating with TCEA (Dixon et al., 2017).

Unfortunately, repeat measurements of the $\delta^{13}C$ and carbon concentrations of the glasses were not possible using SHM-IRMS due to the large amount of material required (> 0.1 g). However, previous studies achieved $\pm 0.21 - 0.49$ ‰ $\delta^{13}C$ and $\pm 8 - 26$ µg g^{-1} CO_2 errors on repeat analyses, which are within the errors on reported values reported here (Macpherson et al., 1999; Mattey et al., 1989; Pineau and Javoy, 1994). The carbon isotope values are much lower than the initial $CaCO_3$ used in the starting material (-14.3 ± 0.7 to -10.2 ± 0.2 vs. -5.43 ± 0.02 to $+1.99 \pm 0.03$ ‰ $\delta^{13}C$). This is likely due to a combination of equilibrium melt-vapor partitioning (e.g., Javoy et al., 1978; Lee et al., 2024; Mattey, 1991; Mattey et al., 1990; Petschnig et al., 2024) and contamination during preparation. This highlights the importance of measuring the isotopic composition of the reference glass rather than assuming it equates to that of the starting composition. Based on spatially separated repeat SIMS measurements our glasses are sufficiently homogeneous for use as reference materials as CO_2 concentrations vary by <10 % (see Supplementary Material) and carbon isotope ratios by < 8 %.

A comparison of the different techniques for H_2O and CO_2 concentration determination are shown in Supplementary Figure S5. In summary, these glasses contain $2026 \pm 34 - 3360 \pm 180$ µg g^{-1} CO_2 as carbonate ions at -14.3 ± 0.7 to -10.2 ± 0.7 ‰ $\delta^{13}C$ and 1.33 ± 0.06 to 2.86 ± 0.06 % g $g^{-1} H_2O$ as molecular H_2O and hydroxyl ions at -101.6 ± 0.9 to -135.7 ± 0.9 ‰ δD (full composition in Table 1).

Table 1 Composition of synthesised glass reference materials.

	Technique	ETNA24	*1s*	ETNA32	*1s*	ETNA36	*1s*
SiO_2 (% g g^{-1})	EPMA	50.43	*0.12*	49.60	*0.12*	48.90	*0.09*
TiO_2 (% g g^{-1})	EPMA	1.78	*0.03*	1.80	*0.03*	1.80	*0.03*
Al_2O_3 (% g g^{-1})	EPMA	17.54	*0.07*	16.15	*0.05*	16.04	*0.08*
FeO_T (% g g^{-1})	EPMA	10.46	*0.07*	8.87	*0.16*	9.90	*0.11*
MnO (% g g^{-1})	EPMA	0.21	*0.02*	0.17	*0.01*	0.17	*0.01*
MgO (% g g^{-1})	EPMA	6.21	*0.06*	6.25	*0.04*	6.23	*0.05*
CaO (% g g^{-1})	EPMA	6.98	*0.04*	10.52	*0.08*	10.36	*0.09*
Na_2O (% g g^{-1})	EPMA	4.08	*0.07*	4.20	*0.06*	4.16	*0.08*
K_2O (% g g^{-1})	EPMA	1.84	*0.02*	1.92	*0.02*	1.89	*0.02*
P_2O_5 (% g g^{-1})	EPMA	0.48	*0.03*	0.53	*0.02*	0.53	*0.02*
Fe^{3+}/Fe_T	EPMA	0.24	*0.07*	0.21	*0.08*	0.20	*0.07*
H_2O (% g g^{-1})	TCEA-IRMS	2.86	*0.06*	1.02	*0.06*	2.30	*0.06*
CO_2 (µg g^{-1})	SHM-IRMS	2300	*69*	3360	*180*	2026	*34*
δD (‰)	TCEA-IRMS	-135.7	*0.9*	-103.9	*0.9*	-101.6	*0.9*
$\delta^{13}C$ (‰)	SHM-IRMS	-14.3	*0.7*	-12.1	*0.2*	-10.2	*0.7*

Notes: Major and minor elements are normalised to volatile-free glass composition.

5 $\delta^{13}C$ SIMS Analysis

5.1 Precision

External and internal precision estimates characterise the improvements in precision gained by our 100-cycle set-up. We demonstrate this improvement using repeat analyses on the ETNA36 reference glass analysed during the February analytical session (Figure 3). External precision is calculated as the standard deviation (σ) around the mean of a large population of analyses. Since the number of cycles conducted on

ETNA36 are limited, we used the sample standard deviation (s) to provide an unbiased best estimate of σ (Figure 3b). To assess consistent external precision, a t-test was conducted for each analysis, comparing the individual s with the best estimate of σ (Figure 3a). No statistically significant differences (all p-values > 0.05; see Supplementary Material) were observed, indicating that external precision remained consistent across all analyses. The improvement in external precision over the 100 cycle analysis was monitored using the cumulative relative sample standard deviation on the mean for each cycle across all analysis of ETNA36 during the February 2024 session (Figure 3a). The external precision stabilises at 45 cycles.

The internal precision characterises the uncertainty on the mean of an individual analysis and is calculated as the relative standard error of the mean of the cycle measurements (RSE; Fitzsimons et al., 2000). RSE is calculated using the standard error of the mean (SEM) = $1\mathrm{s}/\sqrt{\mathrm{n}}$ where 1s is the sample standard deviation and n is the number of analyses and is calculated relative to the sample mean ($\bar{x}$), as $\mathrm{RSE} = \frac{\mathrm{SEM}}{\bar{x}}$. This implies n cycles characterise the mean $\sqrt{\mathrm{n}}$ times more precisely than a single cycle. Figure 3a shows internal precision improves as the number of cycles included in an analysis increase up to 100. Once the number of cycles included in the isotope ratio measurement reaches between 60 to 80, the internal precision drops below 0.5 ‰ 1 RSE (grey shaded area Figure 3a). Towards 100 cycles both the internal and external precision converge towards similar values. At 80 cycles the internal precision is < 0.5 ‰ 1 RSE (blank curves, Figure 3a), and the external precision has also stabilised (orange curve, Figure 3a). For ETNA36, an 80 cycle analysis yields similar precision to a 100 cycle

analysis suggests that a 20% reduction in cycles improves the overall cost-efficiency of the analysis with little loss in reproducibility.

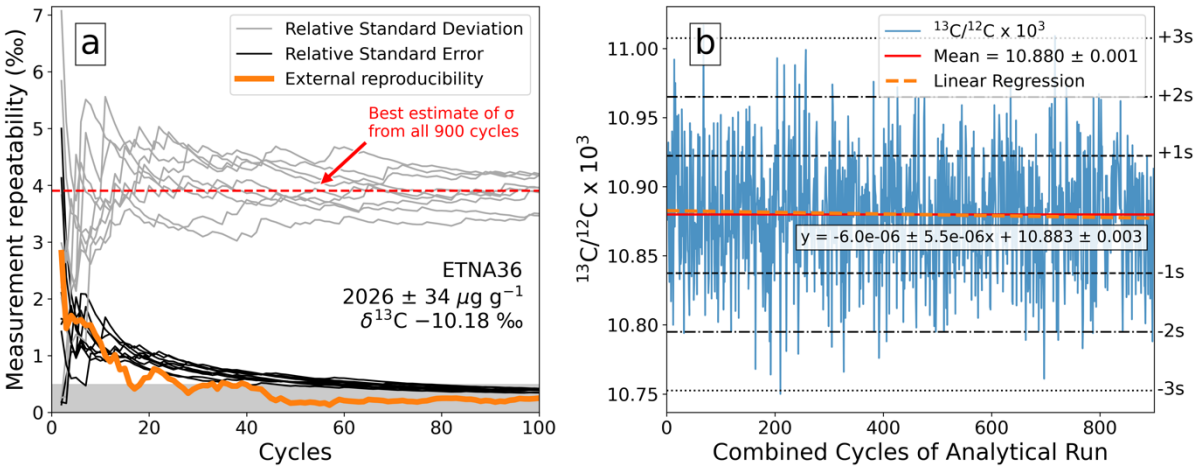

Figure 3. Variation in cumulative relative sample deviation, the cumulative relative standard error of the mean, and the external reproducibility of ETNA36 (a) and the distribution of measurements across all cycles from the February 2024 session (b). The best estimate of the standard deviation (σ) in (a) is taken as the 1s from (b), which represents all measurements throughout the session. The minor slope of measurements across the session is indicated by the low gradient ($-6.0 \times 10^{-6} \pm 5.5 \times 10^{-6}$) and an intercept ($10.8333 \pm 0.003\ ^{13}C/^{12}C \times 10^{3}$) within standard error of the session average ($10.879 \pm 0.001\ ^{13}C/^{12}C \times 10^{3}$), showing negligible drift over the course of the session. The orange line indicates the external precision over the course of an analysis by showing the standard deviation from the mean of the individual sample standard deviations of each analysis of ETNA 36 throughout the run. The grey shaded area in (a) is < 0.5 ‰.

The internal precision of the measurements is dependent on the sensitivity of the set-up, the homogeneity of the analysed material, and surface contamination (Fitzsimons et al., 2000). At low carbon concentrations the standard error is dominated by counting statistics, and samples with significant surface contamination will have decreasing ratios throughout the analysis, which result in less precise measurements

(Marschall and Ludwig, 2004). Our sample preparation minimised carbon contamination, the 300s pre-sputter limits contamination to carbon entering the pit during the analysis, and by controlling the ^{12}C counts with the field aperture we minimised signal from the pit edges where carbon likely enters during analysis. Variations in the field aperture do limit the sensitivity and ultimately the precision of the measurement. Figure 4 shows this variation in two distinct groups of ETNA24 and ETNA36 counts per second for both ^{12}C and ^{13}C. Measurements with higher sensitivity for these glasses, between $5 - 8 \times 10^3$ (^{13}C) and $5 - 8 \times 10^5$ (^{12}C), were conducted with larger field apertures of 28.74 or $31.25\ \mu m^2$, whereas analyses with lower sensitivity were conducted using a field aperture of $20.46\ \mu m^2$. Sample specific attention is therefore required when considering the precision needed when optimising for sensitivity. The approach here was to limit count rates to minimise aging to the electron multiplier measuring ^{12}C, and to limit potential surface contamination from the edges of the beam.

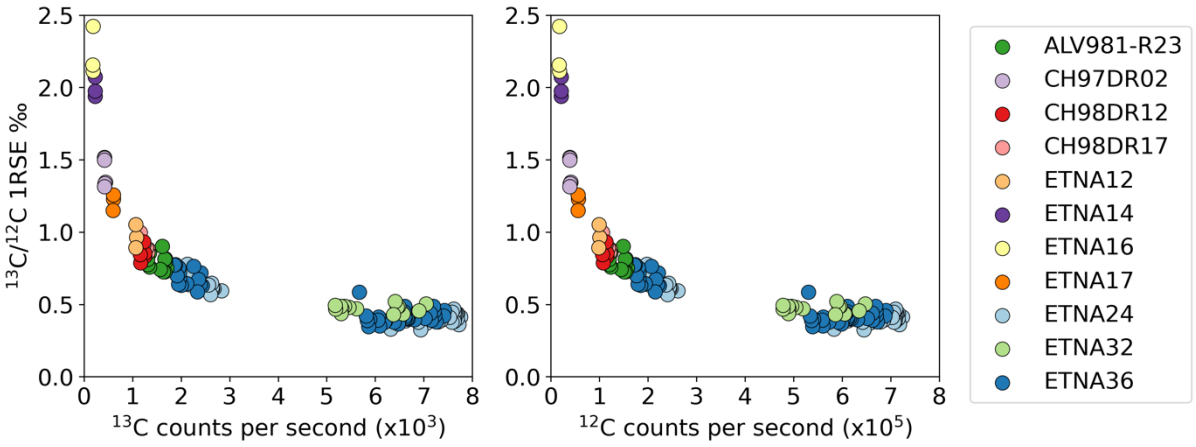

Figure 4. Internal precision of ^{13}C and ^{12}C as a function of counts per second of ^{12}C and ^{13}C. Increasing counts notably improves internal precision. Sensitivity depends on carbon concentration and field aperture. ETNA14, ETNA16, CH97DR02, and ETNA17 have low concentrations ($26.16 - 105.5\ \mu g\ g^{-1}\ CO_2$); ETNA12 and the ocean floor glasses ALV981-R23, CH98DR12, and

CH98DR17 have moderate concentrations ($252 - 535\ \mu g\ g^{-1}\ CO_2$); ETNA24, ETNA32, and ETNA36 have high concentrations ($2026 - 3360\ \mu g\ g^{-1}\ CO_2$; Tables 1–3). Analyses on ETNA24, ETNA32, and ETNA36 used three field apertures (15, 28.75 and $31.5\ \mu m^2$). Multiple field apertures were used to mitigate high ^{12}C count rates to mitigate electron multiplier degradation, which affected sensitivity and precision.

5.2 Drift and Accuracy

Internal drift was identified in each analysis of ETNA36 throughout Run 7 (see Supplementary Materials for run descriptions). The extended analysis times and number of cycles used in this set-up improve repeatability and reproducibility. However, the lengthy analysis times exacerbate any internal drift within a single analysis. ETNA36 in Run 7 had a mild curved surface on a small surface area, which could have affected the primary beam angle of incidence or caused an uneven beam focus, resulting in uneven sputtering and potential variations in the ionisation of the different carbon masses as the pit developed. Figure 5a illustrates the total cycles for all analyses over the course of the run, showing consistent internal drift for individual measurements. Each individual measurements was adjusted using a multiplicative scatter correction based on the average measurement for the total cycles measured throughout the entire run (Figure 5b). Figure 5a shows all cycles measured over the entire run, with each individual measurement coloured separately, and Figure 5b shows the data after the correction. The average value of the entire run was selected since the initial and final $^{13}C/^{12}C$ values were either too high or too low compared the ETNA32 and ETNA36 glasses in the same run. This was confirmed by a normal distribution in the corrected total sessions measurements compared to skewed measurements of the uncorrected data (Figures 5c and 5d), reduction in the slope of the total measurements throughout the entire run

(Figures 5a and 5b), and the alignment of the isotope calibration curve for ETNA24, ETNA32, and ETNA36 measurements compared to the externally constrained $\delta^{13}C$ (Figure 6). Minor slopes were observed in the $^{13}C/^{12}C$ ratio over the course of most analyses, however the slopes did not significantly deviate from zero, and were not corrected.

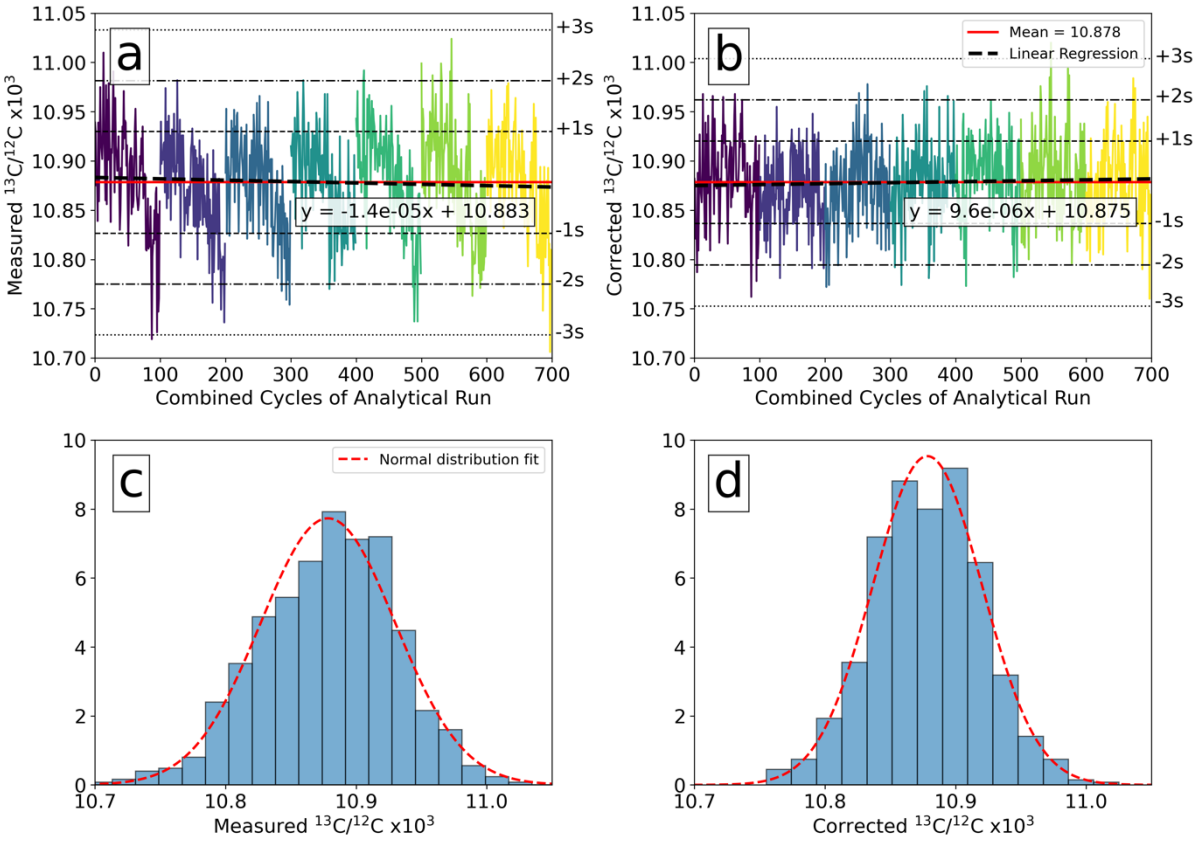

Figure 5. (a) Measured and (b) corrected $^{13}C/^{12}C$ for ETNA36, with colours representing different analyses conducted throughout the total run. Panels (c) and (d) show the distributions of the measured and corrected $^{13}C/^{12}C$, with the normal distribution curves indicating measurement distributions. The measured data are skewed towards higher $^{13}C/^{12}C$values, while the corrected data follow a normal distribution. The corrected data have a lower slope and an intercept closer to the mean.

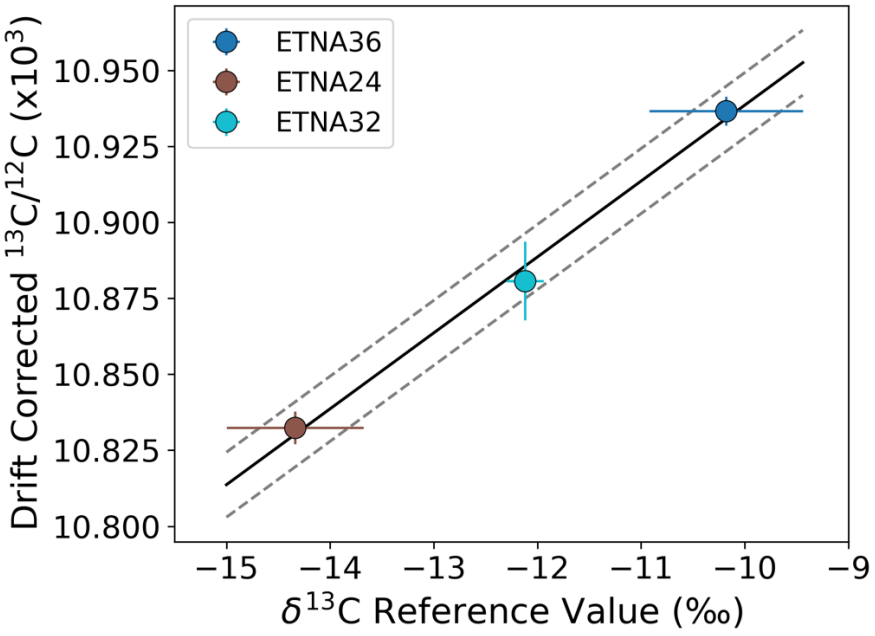

Figure 6. Drift corrected $^{13}C/^{12}C$ ratio verses externally determined $\delta^{13}C$ reference values from SHM-IRMS for Run 7. $\delta^{13}C$ reference values typically have larger errors compared to $^{13}C/^{12}C$ SIMS measurements. The fitted line indicates constant instrumental mass fractionation ($\alpha = 0.9861 \pm 0.0009$). Reference materials, particularly varying in FeO_T, CaO, and H_2O (see Table 1), show no notable matrix effects due to these variations, albeit for 3 glasses with quite similar major element compositions. This plot confirms instrumental mass fractionation was independent of the absolute $^{13}C/^{12}C$ ratio. Dashed line represent the reproducibility of the instrumental fractionation factor.

External drift was identified in three runs by measurements of multiple reference materials through each session. Drift was between 0.04 and 0.11 ‰ per hour and was recognised in long runs between 9 and 20 hours. Typically, two measurements on either two or three of the reference materials were conducted at the start and end of each run, and one measurement was conducted on each reference material every 5 or 6 unknown

measurements, which allowed for the recognition of, and ability to correct for, external drift over the course of a run.

Carbon isotopes currently have no standard materials to assess the accuracy of measurements and are limited to reference materials with sufficient homogeneity. The uncertainties on the external reference materials reported here ($\delta^{13}C \pm 0.18, 0.66, 0.75$ 1s) are relatively large compared to the internal precision of the individual measurements and translate into larger uncertainty on the accuracy of the measurement, when calibrating results to multiple reference materials. The use of an average IMF value determined from a set of reference materials reduces the dependency on a single reference material and the inaccuracy of final $\delta^{13}C$ values. IMF over a single session were calculated using either two or all three reference materials. The use of ETNA32, with higher CO_2 concentration, was added when using a small field aperture, to reduce counts of ^{12}C on the electron multiplier. The reproducibility of the IMF was within 0.34 and 1.13 ‰ 1RSD for all sessions, with the IMF reproducibility of the individual reference materials falling within these range of the overall session for each run (Figure 7). Run 4 and Run 7 were on the same mount rotated 45 degrees, and there was no significant change in the reproducibility to suggest position on the mount is a not significant issue.

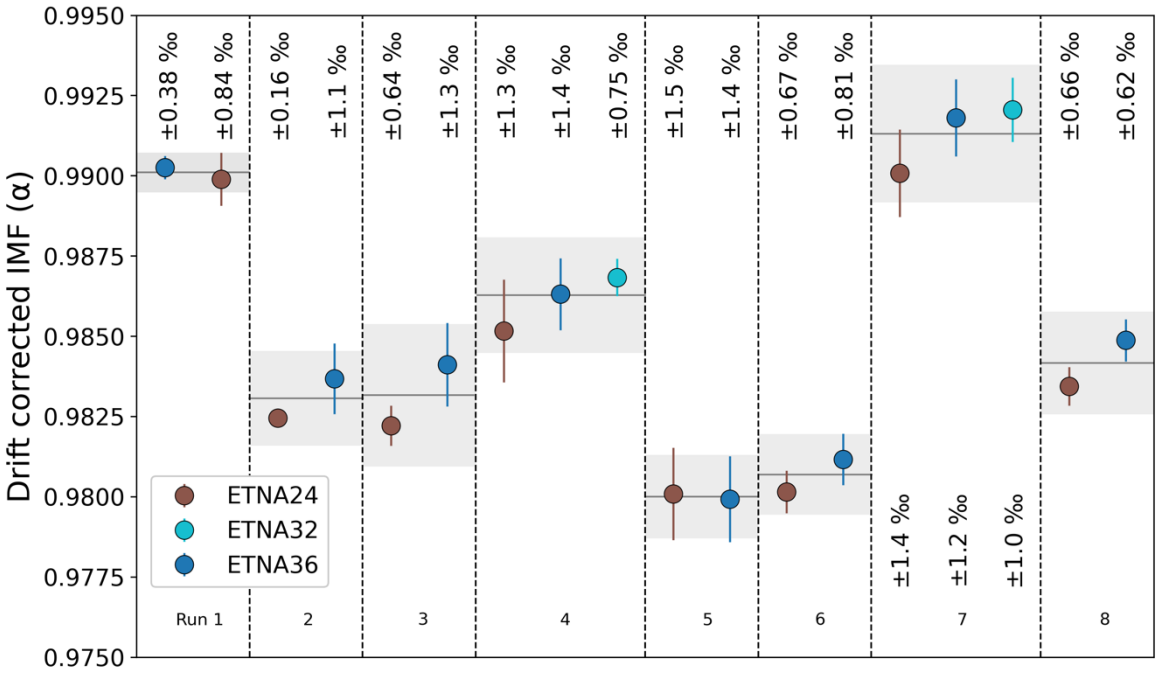

Figure 7. Drift corrected instrumental mass fractionation, α, for each run with reproducibility (2s). Shaded areas are the 2s reproducibility for the average α, which are shown by the black lines, for each run are the combined. Mild offsets between ETNA24, ETNA36, and ETNA32 are likely a result of relatively large uncertainties on the reference materials (Table 1). See Supplementary Material Table 2 for descriptions of the different runs.

5.3 CO_2 reference mass

Cycling the axial mass between collecting carbon masses and a reference mass allows for the simultaneous measurement of carbon isotope ratios and carbon concentration. We considered three reference masses, ^{18}O, $^{28}Si^{2+}$, and ^{30}Si. We did not detect any transmission of $^{28}Si^{2+}$, but transmission of ^{18}O and ^{30}Si were detected. Measurements of ^{12}C on an electron multiplier and ^{30}Si or ^{18}O on the faraday cup resulted in decreasing $^{12}C/^{30}Si$ and $^{12}C/^{18}O$, where the $^{12}C/^{30}Si$ slope was systematically greater than $^{12}C/^{18}O$, with an inconsistent slope throughout the analysis for $^{12}C/^{30}Si$, which becomes steeper after 40 cycles (Figure 8). We recommend using 10 cycles to quantify

the CO_2 concentrations, due to the inconsistent ratios measured for throughout the analysis.

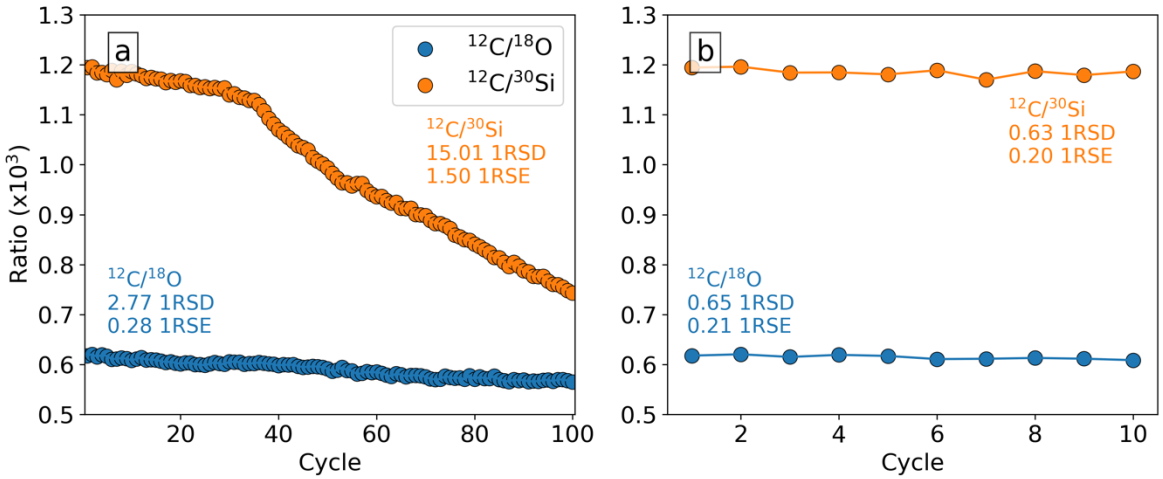

Figure 8. Reference mass ratios per cycle for ^{18}O from the July 2024 session and ^{30}Si from the February 2024 session. Both analyses were conducted on ETNA24. Over 100 cycles, $^{12}C/^{30}Si$ shows (a) large and inconsistent slope for internal drift, while $^{12}C/^{18}O$ only shows a mild and consistent slope for internal drift. These trends are indicated by large 1RSD of 15.01 for $^{12}C/^{30}Si$ and 2.77 for $^{12}C/^{18}O$. While (b) shows the initial 10 cycles mitigate effects from internal drift on both reference masses, markedly lowering both the 1RSD and 1RSE.

Calibration curves rely on multiple, usually ≥ 3, measurements on each reference material that cover the estimated concentration range of the unknown materials being analysed. At 43 minutes per analysis, constructing a robust calibration curve for this SIMS set-up comes with large time and financial costs. Considering issues with significant internal drift over 100 cycles, we use the initial 10 cycles to reduce the associated costs and analytical uncertainties. The reduction of the 1RSD and 1RSE from 100 cycles to 10 cycles, illustrated in Figure 8, shows the benefit of using the first 10 cycles of the measurement for quantifying carbon concentration. Using the initial 10 cycles produces

robust calibration curves (Figure 9). We recommend cycling to axial mass ^{18}O and analysing 10 cycles per analysis so $^{12}C/^{18}O$ can be used to quantify the carbon concentration since it has much lower and consistent drift compared to ^{30}Si.

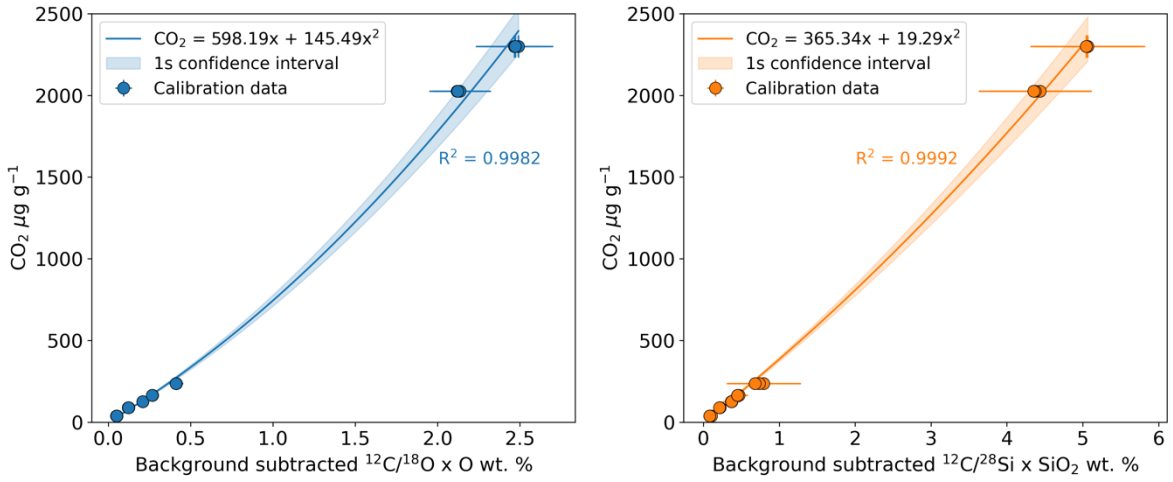

Figure 9. Calibration curves for the ^{18}O reference mass from the July 2024 session and ^{30}Si from the February 2024 session. Orthogonal distance regression (ODR), implemented using SciPy version 1.7.1 (Virtanen et al., 2020), assuming an intercept of 0, was used to fit a quadratic polynomial to the measurement and reference material data, a Jupyter Notebook implementation can be found here in GitHub. This approach accounts for uncertainties in both the reference mass ratio measurements and the CO_2 values of the reference materials. Standard errors of the fitted parameters were used to calculate separate upper and lower 1s confidence intervals, shown by the shaded regions. Error bars on the calibration data points represent 1s of the measurements and reference materials, unless they are smaller than the data point.

5.4 Contamination

The level of contamination in a SIMS analysis depends on the sample preparation, sample storage time, and the analytical set-up. Contamination of carbon is common for both carbon concentration and carbon isotope analyses, which has been attributed to

adsorbed carbon onto the glass surface and inherent carbon in the SIMS vacuum, likely from organic oils used in vacuum pumps (Hauri, 2002; Keppler et al., 2003; Lee et al., 2024). Adsorption of carbon contaminants onto silicate glass surfaces is exacerbated in the presence of H_2O (Baptist and Levy, 1992), and can be collected, along with other volatiles and water soluble compounds, during sample preparation and long storage times (Marschall and Ludwig, 2004). During a SIMS analysis, carbon adsorbed onto the surface may enter the pit from the surrounding surface, and by minimising field apertures the secondary ions from the beam edges can be excluded from collection by the electron multipliers (Marschall and Monteleone, 2015).

We measured the carbon concentration and isotope ratio of the blank by analysing either Icelandic olivine or San Carlos Olivines, which are effectively carbon-free (i.e., carbon saturation is ~ $0.1\ \mu g\ g^{-1}$, Keppler et al., 2003). We obtain an average background either at the beginning and end of a run or taken throughout the run. To show the influence of an average blank measurement, we modelled blank addition to the measurement as a proportion of the measured carbon concentration and isotope ratio from the February run, where the blank had a $\delta^{13}C$ of $-22.55\ ‰ \pm 7.8\ ‰$ 1s at $5.38\ \mu g\ g^{-1}$. Figure 10 shows the influence of the organic blank mixing with a hypothetical sample with a $\delta^{13}C$ of $-5 \pm 0.5\ ‰$, where the CO_2 concentration increases as the proportion of blank in the measurement decreases. The low $\delta^{13}C$ of the organic C background has a negligible effect on samples with high carbon concentrations, however, when CO_2 is $< 200\ \mu g\ g^{-1}$, or 2.75 % of blank in the signal, the correction lies outside of 1s of the analytical error of the sample and without correction the measurement will significantly deviate from the sample composition.

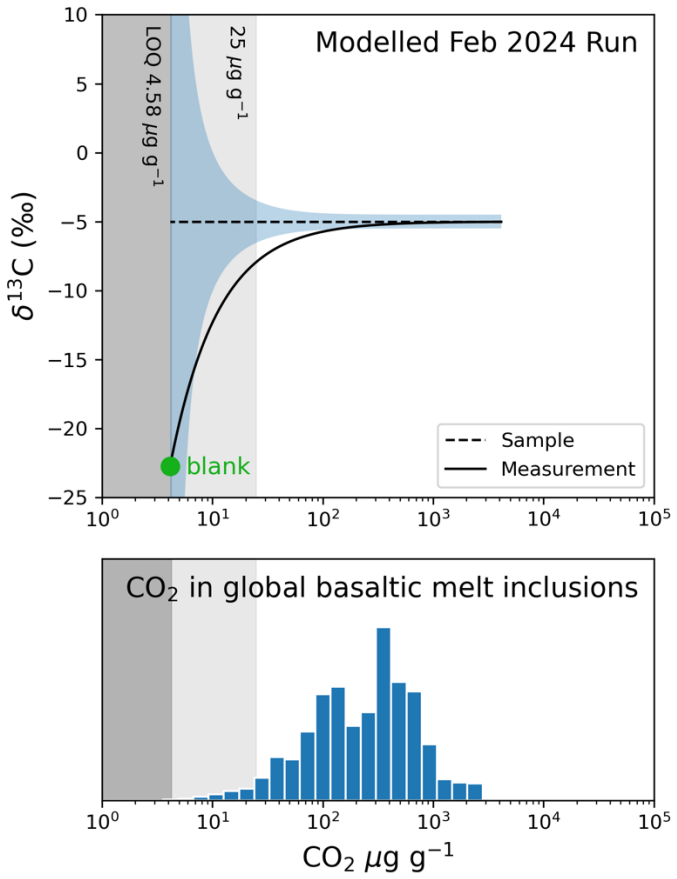

Figure 10 Plots illustrating the effect of the blank mixing with the sample for the total measurement signal in this study, compared to a global dataset for CO_2 in basaltic melt inclusions. The blue shaded area represents the propagated error of the corrected sample, accounting for errors from both the blank and hypothetical sample. The dark grey shaded area indicates CO_2 concentrations below the limit of quantification (LOQ = 4.58 $\mu g\ g^{-1}$ CO_2), and the light grey is at 25 $\mu g\ g^{-1}$ CO_2, where errors begin to increase rapidly and may no longer yield geologically useful information (Figure 1). The measurement concentration is the proportion of sample to blank and a hypothetical $\delta^{13}C$ of -5.00 ± 0.50 ‰ 1s, while the blank has a CO_2 concentration of $4.14^{+0.13}_{-0.12}$ $\mu g\ g^{-1}$ and a $\delta^{13}C$ of -22.7 ± 7.1 ‰ 1s total error. The global CO_2 basaltic melt inclusion dataset is from Figure 5 in Matthews et al. (2021).

We use equations (3) and (4) to correct our SIMS measurements for the influence of the organic blank signal. We constrained the carbon concentration of the

measurement and blank, n_T and n_b, by averaging non-background corrected measurements of the blank olivine, and the measured isotope ratio for the blank and sample for δ_T and δ_b. After applying this correction, for the February 2024 run, we observed results shifting towards higher values, with corrections exceeding 2.00 ‰ for $\delta^{13}C$, and measurements with significantly higher $\delta^{13}C$ values requiring larger corrections. We caution that measurements without blank corrections can produce measurement trends resembling fractional degassing trends under equilibrium conditions (Figure 1). Therefore, blank corrections are critical to ensure accurate interpretations of natural data, and can potentially explain the carbon isotope ratio trend observed by Hauri (2002).

6 Application to basaltic glasses

The overwhelming majority of published carbon isotope ratio measurements of basaltic glasses are currently from bulk samples. The first reported SIMS analyses of carbon isotope ratios in basaltic melts by Hauri (2002) and Hauri et al. (2002) used bulk analyses on a natural basaltic glass, ALV981-R23 from the East Pacific Rise, as a reference material. Reproducibility of CO_2 and $\delta^{13}C$ measurements on submarine glasses has been a systematic analytical issue for decades (Pineau and Javoy, 1983), and incrementally step-heated manometry (SHM) was introduced to address this issue (Macpherson et al., 1999). SHM followed by IRMS has the advantage of separating low temperature carbon contamination from high temperature magmatic carbon, providing both concentration and isotope ratios (Aubaud, 2022; Macpherson et al., 1999).

We analysed using SIMS the ALV981-R23 glass from the East Pacific Rise, which was used by Hauri (2002) and Hauri et al. (2002) and analysed by bulk and *in situ* (FTIR)

methods (Des Marais, 1986; Fine and Stolper, 1986; Macpherson et al., 1999; Pineau and Javoy, 1983). SHM studies by Des Marais (1986) and Macpherson et al. (1999) measured significantly lower CO_2 concentrations (436 and 405.6 ± 8 vs. $645\ \mu g\ g^{-1}$)) and lower $\delta^{13}C$ ($-5.60\ \pm\ 0.1$ and -5.7 ± 0.41 vs. -8.6 ‰) than the single-step pyrolysis study of Pineau and Javoy (1983) for ALV981-R23. This mismatch highlights the importance of step-heating vs. single-step pyrolysis in removing the absorbed carbon: therefore, the Pineau and Javoy (1983) results are not discussed further.

The *in situ* SIMS measurements presented here yield systematically lower carbon concentrations (up to $\sim 120\ \mu g\ g^{-1}$) and higher carbon isotope ratios (up to +4 ‰) compared to previous bulk measurements for all glasses measured (Supplementary Material and Figure 11). This contrasts with Hahm et al. (2012), who compared SHM and SIMS CO_2 concentrations (but not isotope ratios) on basalts from the Lau basin and obtained results within 87 $\mu g\ g^{-1}$ for each other and both over and underestimations. The discrepancy we observe could be due to inhomogeneity within the natural samples, as different glass chips were used for SIMS and SHM. Alternatively, there could be mild contamination of CO_2 in the bulk analyses that has a low carbon isotope ratio. Des Marais (1986) and Macpherson et al. (1999) only include carbon released above $635°C$, and 1000°C, respectively, meaning organic contamination from handling and sample preparation are not potential sources of contamination. Carbon release from vesicles at intermediate temperatures ($\sim 800 - 1000°C$) could be influencing the SHM results, explaining the difference in CO_2 concentrations. However, vesicle carbon typically has an isotopically higher carbon isotope ratio than the glass due to isotopic fractionation (Aubaud, 2022) and hence cannot explain the difference in $\delta^{13}C$. It could be that the blank

during SHM has been underestimated, which would cause both a higher CO_2 concentration and lower carbon isotope ratio. Without carbon isotope data from smaller heat step increments it is unfortunately not possible to identify the cause. Alternatively, given the water contents of these natural glasses are lower than the standards (< 0.4 vs. 1-3 % g g^{-1}), this could contribute to the mismatch (Moussallam et al., 2024).

Repeat points on the natural glasses show isotope heterogeneity, with $\delta^{13}C$ ranging by ~ 2 to 3 ‰ on a single chip (Table 2 and Figure 11). This may have been driven by vesicles close to the polished surface, resulting in fractionation between ^{12}C and ^{13}C that has been captured during quenching. This heterogeneity likely contributed to the low precision achieved when ALV981-R23 was used as a reference material in the pioneering work by Hauri (2002) and Hauri et al. (2002).

Carbon concentrations varied between sessions, which used ^{28}Si and ^{18}O as reference materials. The AVL981-R23 glass have two populations of CO_2 concentration, a low group between $282.0^{+9.5}_{-9.4}$ µg g^{-1} (n = 4), and a high group at 343^{+14}_{-14} µg g^{-1} (n = 7), 1s. The low group was measured in February 2024 using ^{28}Si as a reference mass, whereas the high group was measured in July 2024 using ^{18}O as a reference mass. The agreement with the FTIR CO_2 concentration of 347 ± 15 µg g^{-1} from Fine and Stolper (1986) suggesting ^{18}O is the superior reference mass.

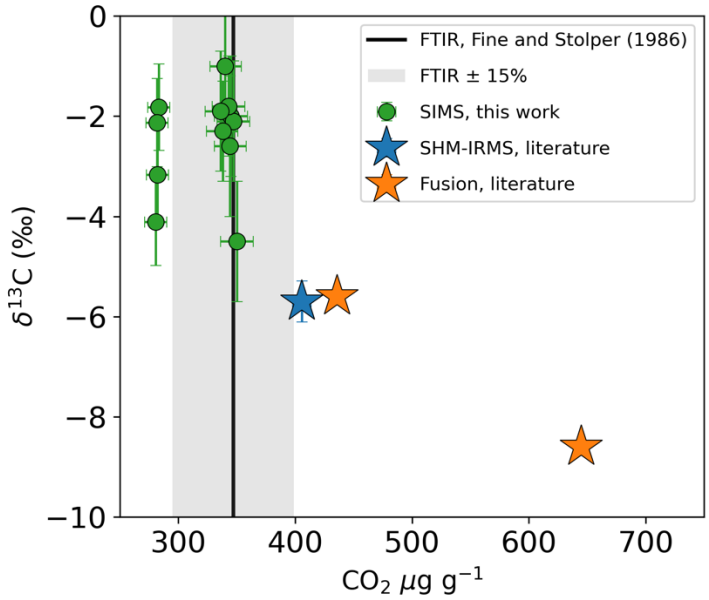

Figure 11. Glasses from the East Pacific Rise (ALV981-R23) analysed by SIMS (small symbols) and bulk methods (large stars), by SHM-IRMS and Fusion (Des Marais, 1986; Macpherson et al., 1999; Pineau and Javoy, 1983) and carbon concentration by FTIR (Fine and Stolper, 1986). SIMS analyses presented here have lower carbon concentration compared to bulk pyrolysis methods, however agree with FTIR results from Fine and Stolper (1986). The two populations of SIMS results use separate reference masses, with the lower concentrations using ^{30}Si and higher concentrations using ^{18}O. All errors plotted here are 1s, no errors were reported for the fusion bulk analyses, otherwise unseen errors are smaller than the point.

We also analysed synthetic basaltic glasses with varying concentrations to demonstrate the usefulness of the SIMS set-up at low concentrations (Hughes et al., 2018, Table S3 and Figure 12). Only ETNA17 significantly deviated from the measurements conducted on the Cameca 4f (Table SX), whereas all other measurements were within 1s error, demonstrating the usefulness of the approach. The significant variation between ETNA17 reported here and using the Cameca 4f is possibly due to sample heterogeneity between different glass chips (Figure 12).

ETNA16, the sample with lowest carbon concentrations, ranging between $28.16^{+0.92}_{-0.92}$ and $29.66^{+0.98}_{-0.97}$ µg g^{-1} 1s, yielded final δ^{13}C measurement precision between 3.0 and 3.3 ‰. Our highest limit of quantification (LOQ) was 19.16 µg g^{-1}, which is close to the concentrations measured on ETNA16. We caution analysts targeting carbon concentrations lower than 25 µg g^{-1} using SIMS, unless there are improvements in reducing the carbon blank, given the reduction in precision when error propagation is performed on the blank corrected measurements (Figure 10). Given the substantial fractionation at low carbon concentrations in basaltic melts (Figure 1), the precision reported here at 25 µg g^{-1} could still be geologically useful, depending on the application.

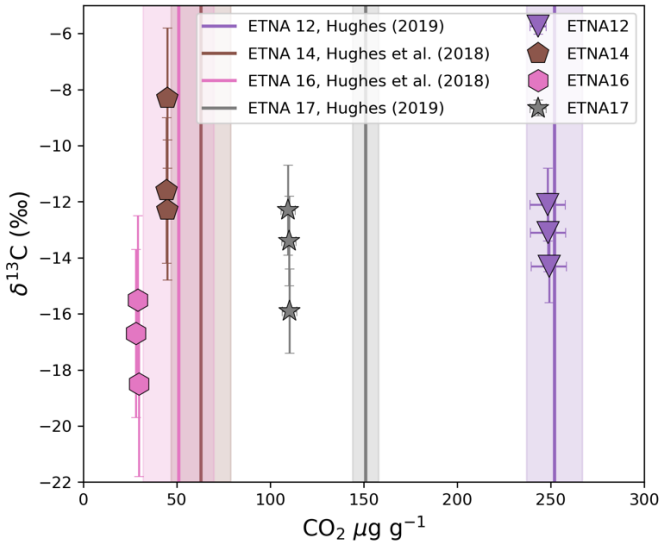

Figure 12. SIMS analyses of synthetic ETNA glasses with low to moderate carbon concentrations (Hughes, 2019; Hughes et al., 2018, collected on a Cameca 4f). All errors, including the shaded regions for SIMS data, are shown as 1s. Concentrations from the presented SIMS analyses generally align with previous findings, though systematically lower. Notably, the sample ETNA17 shows significantly lower concentrations, exceeding the reported errors, suggesting potential sample heterogeneity.

7 Conclusion

We have addressed key challenges that previously inhibited the routine adoption of *in situ* carbon isotope analysis by SIMS. Namely, we focused on accurately characterising the dissolved carbon component in reference materials, improved secondary ion transmission without substantial surface contamination at high precision, increased total analysis time with a larger number of cycles, and a method to characterise and correct for the carbon blank.

We have developed a workflow for producing and characterising homogeneous reference materials suitable for *in situ* carbon isotope analyses in basaltic glasses. Our approach, using SHM-IRMS, which effectively addresses carbon contamination issues common in the bulk characterisation of carbon concentration and isotope analyses in basaltic glasses. By using a graphite-free assembly in an IHPV apparatus, we produced homogenous $^{13}C/^{12}C$ ratios in the synthetic glasses by limiting potential ^{12}C infiltration from a graphite furnace (Brooker et al., 1998). A current limitation for *in situ* carbon isotope ratio analyses of basaltic glasses is the limited number of suitable reference materials across a range of carbon concentrations, especially at low and carbon-free concentrations. The addition of δD and H_2O characterisation in our reference materials allows for multiple isotope systems to be explored simultaneously. We hope this workflow will be adopted by the secondary ion probe community to address this gap.

This improved SIMS set-up used at the NEIMF at WHOI reduced analytical uncertainty by at least a factor of 3 compared to previous work, although at the expense of total analysis time and a larger pit size (40 µm diameter). At high carbon

concentrations, the resulting uncertainties are comparable or approaching those of bulk determinations of basaltic glasses and can be applied to glass at low carbon concentrations, down to 25 μg g^{-1}, depending on the required precision. This significantly reduces the amount of required material and opens avenues for work on the tens of micron-scale. Initial results of SIMS measurements conducted on natural glasses with SHM-IRMS highlight the need for a standardised and robust approach to measuring bulk samples. Future improvements on the approach described here will centre around the reduction of carbon blanks, which will allow for the use of a larger field aperture which will significantly improve transmission.

We see this, or a similar approach, as an essential tool for understanding carbon storage and recycling throughout the mantle, linking the behaviour and volatility of magmatic systems linked to carbon degassing processes, and tracing how basaltic melts deliver carbon from mantle and lithospheric reservoirs to the atmosphere.

The reference materials presented here are available at the Northeast National Ion Microprobe Facility at WHOI and upon request to the corresponding authors.

Acknowledgements

We would like to thank S Remmelzwall for helping to the clean the SHC sample; D Hilton, who passed away in 2018, for providing the ALV981-R23 sample; A Nederbragt for analysing the $\delta^{13}C$ of the $CaCO_3$; J Craven and R Hinton for their assistance at the NERC ion microprobe facility at the University of Edinburgh, UK (IMF560/0515); S Kearns and B Buse for their assistance with the electron probe at the University of Bristol, UK; F Holtz

for providing access to the IHPV lab at the Leibniz University of Hannover, Germany. A special thank you goes to H Mader, who passed away in 2022, for all her help and support of this work during Hughes' PhD thesis. JS and OS acknowledge funding from UKRI NERC grants NE/T012455/1 and NE/V011383/1. ECH was supported by a NERC GW4+ DTP studentship (NE/L002434/1) and is thankful for the support and additional funding from CASE partner Te Pū Ao | GNS Science, Aotearoa New Zealand: parts of this paper are taken from Hughes' thesis (2019). GK and ECH are supported by the New Zealand Ministry of Business, Innovation and Employment (MBIE) through the Hazards and Risk Management (Strategic Science Investment Fund, contract C05X1702). JB is supported be a Royal Society Research Professorship (RP\R1\201048).

References

Aubaud, C., 2022. Carbon stable isotope constraints on CO2 degassing models of ridge, hotspot and arc magmas. Chem. Geol. 605, 120962. https://doi.org/10.1016/j.chemgeo.2022.120962

Baptist, R., Levy, F., 1992. Carbon dioxide adsorption on glass. Vacuum 43, 213–214. https://doi.org/10.1016/0042-207X(92)90263-V

Barker, S., Greaves, M., Elderfield, H., 2003. A study of cleaning procedures used for foraminiferal Mg/Ca paleothermometry. Geochem. Geophys. Geosystems 4, 2003GC000559. https://doi.org/10.1029/2003GC000559

Berndt, J., Liebske, C., Holtz, F., Freise, M., Nowak, M., Ziegenbein, D., Hurkuck, W., Koepke, J., 2002. A combined rapid-quench and H_2-membrane setup for internally heated pressure vessels: Description and application for water solubility in basaltic melts. Am. Mineral. 87, 1717–1726. https://doi.org/10.2138/am-2002-11-1222

Blundy, J., Cashman, K., 2008a. Petrologic Reconstruction of Magmatic System Variables and Processes. Rev. Mineral. Geochem. 69, 179–239. https://doi.org/10.2138/rmg.2008.69.6

Blundy, J., Cashman, K., 2008b. Petrologic Reconstruction of Magmatic System Variables and Processes. Rev. Mineral. Geochem. 69, 179–239. https://doi.org/10.2138/rmg.2008.69.6

Brand, W.A., Coplen, T.B., Vogl, J., Rosner, M., Prohaska, T., 2014. Assessment of international reference materials for isotope-ratio analysis (IUPAC Technical Report). Pure Appl. Chem. 86, 425–467. https://doi.org/10.1515/pac-2013-1023

Brooker, R., Holloway, J.R., Hervig, R., 1998. Reduction in piston-cylinder experiments; the detection of carbon infiltration into platinum capsules. Am. Mineral. 83, 985–994. https://doi.org/10.2138/am-1998-9-1006

Coplen, T.B., 2011. Guidelines and recommended terms for expression of stable-isotope-ratio and gas-ratio measurement results. Rapid Commun. Mass Spectrom. 25, 2538–2560. https://doi.org/10.1002/rcm.5129

Deines, P., 1970. The carbon and oxygen isotopic composition of carbonates from the Oka carbonatite complex, Quebec, Canada. Geochim. Cosmochim. Acta 34, 1199–1225. https://doi.org/10.1016/0016-7037(70)90058-X

Des Marais, D.J., 1986. Carbon abundance measurements in oceanic basalts: the need for a consensus. Earth Planet. Sci. Lett. 79, 21–26. https://doi.org/10.1016/0012-821X(86)90036-1

Dixon, J.E., Bindeman, I.N., Kingsley, R.H., Simons, K.K., Le Roux, P.J., Hajewski, T.R., Swart, P., Langmuir, C.H., Ryan, J.G., Walowski, K.J., Wada, I., Wallace, P.J., 2017. Light Stable Isotopic Compositions of Enriched Mantle Sources: Resolving the Dehydration Paradox. Geochem. Geophys. Geosystems 18, 3801–3839. https://doi.org/10.1002/2016GC006743

Donovan, J.J., Tingle, T.N., 1996. An Improved Mean Atomic Number Background Correction for Quantitative Microanalysis. Microsc. Microanal. 2, 1–7. https://doi.org/10.1017/S1431927696210013

Exley, R.A., Mattey, D.P., Clague, D.A., Pillinger, C.T., 1986. Carbon isotope systematics of a mantle “hotspot”: a comparison of Loihi Seamount and MORB glasses. Earth Planet. Sci. Lett. 78, 189–199. https://doi.org/10.1016/0012-821X(86)90060-9

Fine, G., Stolper, E., 1986. Dissolved carbon dioxide in basaltic glasses: concentrations and speciation. Earth Planet. Sci. Lett. 76, 263–278. https://doi.org/10.1016/0012-821X(86)90078-6

Fine, G., Stolper, E., 1985. The speciation of carbon dioxide in sodium aluminosilicate glasses. Contrib. Mineral. Petrol. 91, 105–121. https://doi.org/10.1007/BF00377759

Fitzsimons, I.C.W., Harte, B., Chinn, I.L., Gurney, J.J., Taylor, W.R., 1999. Extreme chemical variation in complex diamonds from George Creek, Colorado: a SIMS study of carbon isotope composition and nitrogen abundance. Mineral. Mag. 63, 857–878. https://doi.org/10.1180/002646199548970

Fitzsimons, I.C.W., Harte, B., Clark, R.M., 2000. SIMS stable isotope measurement: counting statistics and analytical precision. Mineral. Mag. 64, 59–83. https://doi.org/10.1180/002646100549139

Gelwicks, J.T., Hayes, J.M., 1990. Carbon-isotopic analysis of dissolved acetate. Anal. Chem. 62, 535–539. https://doi.org/10.1021/ac00204a021

Gonfiantini, R., 1984. Advisory Group Meeting on Stable Isotope Reference Samples for Geochemical and Hydrological Investigations. International Atomic Energy Agency, Vienna, Austria.

Hahm, D., Hilton, D.R., Castillo, P.R., Hawkins, J.W., Hanan, B.B., Hauri, E.H., 2012. An overview of the volatile systematics of the Lau Basin – Resolving the effects of source variation, magmatic degassing and crustal contamination. Geochim. Cosmochim. Acta 85, 88–113. https://doi.org/10.1016/j.gca.2012.02.007

Hauri, E., 2002. SIMS analysis of volatiles in silicate glasses, 2: isotopes and abundances in Hawaiian melt inclusions. Chem. Geol. 183, 115–141. https://doi.org/10.1016/S0009-2541(01)00374-6

Hauri, E., Wang, J., Dixon, J.E., King, P.L., Mandeville, C., Newman, S., 2002. SIMS analysis of volatiles in silicate glasses 1. Calibration, matrix effects and comparisons with FTIR. Chem. Geol.

Hemingway, J.D., Galy, V.V., Gagnon, A.R., Grant, K.E., Rosengard, S.Z., Soulet, G., Zigah, P.K., McNichol, A.P., 2017. Assessing the Blank Carbon Contribution, Isotope Mass Balance, and Kinetic Isotope Fractionation of the Ramped Pyrolysis/Oxidation Instrument at NOSAMS. Radiocarbon 59, 179–193. https://doi.org/10.1017/RDC.2017.3

Hoffman, D.W., Rasmussen, C., 2022. Absolute Carbon Stable Isotope Ratio in the Vienna Peedee Belemnite Isotope Reference Determined by ^{1}H NMR Spectroscopy. Anal. Chem. 94, 5240–5247. https://doi.org/10.1021/acs.analchem.1c04565

Hudak, M.R., Bindeman, I.N., Watkins, J.M., Lowenstern, J.B., 2022. Hydrogen isotope behavior during rhyolite glass hydration under hydrothermal conditions. Geochim. Cosmochim. Acta 337, 33–48. https://doi.org/10.1016/j.gca.2022.09.032

Hughes, E.C., 2019. Microanalyical Techniques and Experimental Studies of the Volatile and fO2 History of Magmas using Melt Inlcusions. University of Bristol.

Hughes, E.C., Buse, B., Kearns, S.L., Blundy, J.D., Kilgour, G., Mader, H.M., Brooker, R.A., Balzer, R., Botcharnikov, R.E., Di Genova, D., Almeev, R.R., Riker, J.M., 2018. High spatial resolution analysis of the iron oxidation state in silicate glasses using the electron probe. Am. Mineral. 103, 1473–1486. https://doi.org/10.2138/am-2018-6546CCBY

Javoy, M., Pineau, F., 1991. The volatiles record of a "popping" rock from the Mid-Atlantic Ridge at 14°N: chemical and isotopic composition of gas trapped in the vesicles. Earth Planet. Sci. Lett. 107, 598–611. https://doi.org/10.1016/0012-821X(91)90104-P

Javoy, M., Pineau, F., Iiyama, I., 1978. Experimental determination of the isotopic fractionation between gaseous CO2 and carbon dissolved in tholeiitic magma: A preliminary study. Contrib. Mineral. Petrol. 67, 35–39. https://doi.org/10.1007/BF00371631

Jendrzejewski, N., Trull, T.W., Pineau, F., Javoy, M., 1997. Carbon solubility in Mid-Ocean Ridge basaltic melt at low pressures (250–1950 bar). Chem. Geol. 138, 81–92. https://doi.org/10.1016/S0009-2541(96)00176-3

Jenkyns, H.C., Gale, A.S., Corfield, R.M., 1994. Carbon- and oxygen-isotope stratigraphy of the English Chalk and Italian Scaglia and its palaeoclimatic significance. Geol. Mag. 131, 1–34. https://doi.org/10.1017/S0016756800010451

Keppler, H., Wiedenbeck, M., Shcheka, S.S., 2003. Carbon solubility in olivine and the mode of carbon storage in the Earth's mantle. Nature 424, 414–416. https://doi.org/10.1038/nature01828

King, P.L., Vennemann, T.W., Holloway, J.R., Hervig, R.L., Lowenstern, J.B., Forneris, J.F., 2002. Analytical techniques for volatiles: A case study using intermediate (andesitic) glasses. Am. Mineral. 87, 1077–1089. https://doi.org/10.2138/am-2002-8-904

Le Voyer, M., Deloule, E., Kelley, K.A., Cartigny, P., Cottrell, E., Hauri, E.H., 2014. Ion microprobe analyses of carbon isotope ratios in MORB. Presented at the Goldschmidt, Sacramento, California, USA.

Lee, H., Moussallam, Y., Rose-Koga, E., Piani, L., Villeneuve, J., Bouden, N., Gurenko, A., Monteleone, B., Gaetani, G., 2024. High–precision determination of carbon stable isotope in silicate glasses by secondary ion mass spectrometry: Evaluation of international reference materials. Chem. Geol. 122428. https://doi.org/10.1016/j.chemgeo.2024.122428

Lockyer, N.P., Aoyagi, S., Fletcher, J.S., Gilmore, I.S., Van Der Heide, P.A.W., Moore, K.L., Tyler, B.J., Weng, L.-T., 2024. Secondary ion mass spectrometry. Nat. Rev. Methods Primer 4, 32. https://doi.org/10.1038/s43586-024-00311-9

Macpherson, C., Mattey, D., 1994. Carbon isotope variations of CO2 in Central Lau Basin basalts and ferrobasalts. Earth Planet. Sci. Lett. 121, 263–276. https://doi.org/10.1016/0012-821X(94)90072-8

Macpherson, C.G., Hilton, D.R., Newman, S., Mattey, D.P., 1999. CO2, 13C/12C and H2O variability in natural basaltic glasses: a study comparing stepped heating and FTIR spectroscopic techniques. Geochim. Cosmochim. Acta 63, 1805–1813. https://doi.org/10.1016/S0016-7037(99)00124-6

Marschall, H.R., Ludwig, T., 2004. The low-boron contest: minimising surface contamination and analysing boron concentrations at the ng/g-level by secondary ion mass spectrometry. Mineral. Petrol. 81, 265–278. https://doi.org/10.1007/s00710-004-0037-5

Marschall, H.R., Monteleone, B.D., 2015. Boron Isotope Analysis of Silicate Glass with Very Low Boron Concentrations by Secondary Ion Mass Spectrometry. Geostand. Geoanalytical Res. 39, 31–46. https://doi.org/10.1111/j.1751-908X.2014.00289.x

Mattey, D.P., 1991. Carbon dioxide solubility and carbon isotope fractionation in basaltic melt. Geochim. Cosmochim. Acta 55, 3467–3473. https://doi.org/10.1016/0016-7037(91)90508-3

Mattey, D.P., Carr, R.H., Wright, I.P., Pillinger, C.T., 1984. Carbon isotopes in submarine basalts. Earth Planet. Sci. Lett. 70, 196–206. https://doi.org/10.1016/0012-821X(84)90005-0

Mattey, D.P., Exley, R.A., Pillinger, C.T., 1989. Isotopic composition of CO2 and dissolved carbon species in basalt glass. Geochim. Cosmochim. Acta 53, 2377–2386. https://doi.org/10.1016/0016-7037(89)90359-1

Mattey, D.P., Taylor, W.R., Green, D.H., Pillinger, C.T., 1990. Carbon isotopic fractionation between CO2 vapour, silicate and carbonate melts: an experimental study to 30 kbar. Contrib. Mineral. Petrol. 104, 492–505. https://doi.org/10.1007/BF01575626

Matthews, S., Shorttle, O., Maclennan, J., Rudge, J.F., 2021. The global melt inclusion C/Ba array: Mantle variability, melting process, or degassing? Geochim. Cosmochim. Acta 293, 525–543. https://doi.org/10.1016/j.gca.2020.09.030

Meija, J., Coplen, T.B., Berglund, M., Brand, W.A., De Bièvre, P., Gröning, M., Holden, N.E., Irrgeher, J., Loss, R.D., Walczyk, T., Prohaska, T., 2016. Isotopic

compositions of the elements 2013 (IUPAC Technical Report). Pure Appl. Chem. 88, 293–306. https://doi.org/10.1515/pac-2015-0503

Morizet, Y., Brooker, R.A., Iacono-Marziano, G., Kjarsgaard, B.A., 2013. Quantification of dissolved CO2 in silicate glasses using micro-Raman spectroscopy. Am. Mineral. 98, 1788–1802. https://doi.org/10.2138/am.2013.4516

Moussallam, Y., Towbin, W.H., Plank, T., Bureau, H., Khodja, H., Guan, Y., Ma, C., Baker, M.B., Stolper, E.M., Naab, F.U., Monteleone, B.D., Gaetani, G.A., Shimizu, K., Ushikubo, T., Lee, H.J., Ding, S., Shi, S., Rose-Koga, E.F., 2024. ND70 Series Basaltic Glass Reference Materials for Volatile Element (H_2O , CO_2 , S, Cl, F) Measurement and the C Ionisation Efficiency Suppression Effect of Water in Silicate Glasses in SIMS. Geostand. Geoanalytical Res. ggr.12572. https://doi.org/10.1111/ggr.12572

Mysen, B., 2017. Experimental, in-situ carbon solution mechanisms and isotope fractionation in and between (C–O–H)-saturated silicate melt and silicate-saturated (C–O–H) fluid to upper mantle temperatures and pressures. Earth Planet. Sci. Lett. 459, 352–361. https://doi.org/10.1016/j.epsl.2016.11.051

Mysen, B., 2016. Experimentally-determined carbon isotope fractionation in and between methane-bearing melt and fluid to upper mantle temperatures and pressures. Earth Planet. Sci. Lett. 445, 28–35. https://doi.org/10.1016/j.epsl.2016.04.004

Nielsen, C.H., Sigurdsson, H., 1981. Quantitative methods for electron microprobe analysis of sodium in natural and synthetic glasses. Am. Mineral. 66, 547–552.

Nolan, G.S., Bindeman, I.N., 2013. Experimental investigation of rates and mechanisms of isotope exchange (O, H) between volcanic ash and isotopically-labeled water. Geochim. Cosmochim. Acta 111, 5–27. https://doi.org/10.1016/j.gca.2013.01.020

Petschnig, P., Schmidt, M.W., Kueter, N., Sartori, G., Bernasconi, S.M., 2024. An almost universal CO2 - CO32− carbon isotope fractionation function for high temperatures. Earth Planet. Sci. Lett. 627, 118552. https://doi.org/10.1016/j.epsl.2023.118552

Pineau, F., Javoy, M., 1994. Strong degassing at ridge crests: The behaviour of dissolved carbon and water in basalt glasses at 14°N, Mid-Atlantic Ridge. Earth Planet. Sci. Lett. 123, 179–198. https://doi.org/10.1016/0012-821X(94)90266-6

Pineau, F., Javoy, M., 1983. Carbon isotopes and concentrations in mid-oceanic ridge basalts. Earth Planet. Sci. Lett. 62, 239–257. https://doi.org/10.1016/0012-821X(83)90087-0

Pineau, F., Javoy, M., Bottinga, Y., 1976. 13C/12C ratios of rocks and inclusions in popping rocks of the Mid-Atlantic Ridge and their bearing on the problem of isotopic composition of deep-seated carbon. Earth Planet. Sci. Lett. 29, 413–421. https://doi.org/10.1016/0012-821X(76)90146-1

Qi, H., Coplen, T.B., Gehre, M., Vennemann, T.W., Brand, W.A., Geilmann, H., Olack, G., Bindeman, I.N., Palandri, J., Huang, L., Longstaffe, F.J., 2017. New biotite and muscovite isotopic reference materials, USGS57 and USGS58, for δ2H measurements–A replacement for NBS 30. Chem. Geol. 467, 89–99. https://doi.org/10.1016/j.chemgeo.2017.07.027

Swart, P.K., Grady, M.M., Pillinger, C.T., 1983. A method for the identification and elimination of contamination during carbon isotopic analyses of extraterrestrial samples. Meteoritics 18, 137–154. https://doi.org/10.1111/j.1945-5100.1983.tb00584.x

Taracsák, Z., Hartley, M.E., Burgess, R., Edmonds, M., Iddon, F., Longpré, M.-A., 2019. High fluxes of deep volatiles from ocean island volcanoes: Insights from El Hierro, Canary Islands. Geochim. Cosmochim. Acta 258, 19–36. https://doi.org/10.1016/j.gca.2019.05.020

Virtanen, P., Gommers, R., Oliphant, T.E., Haberland, M., Reddy, T., Cournapeau, D., Burovski, E., Peterson, P., Weckesser, W., Bright, J., Van Der Walt, S.J., Brett, M., Wilson, J., Millman, K.J., Mayorov, N., Nelson, A.R.J., Jones, E., Kern, R., Larson, E., Carey, C.J., Polat, İ., Feng, Y., Moore, E.W., VanderPlas, J., Laxalde, D., Perktold, J., Cimrman, R., Henriksen, I., Quintero, E.A., Harris, C.R., Archibald, A.M., Ribeiro, A.H., Pedregosa, F., Van Mulbregt, P., SciPy 1.0 Contributors, Vijaykumar, A., Bardelli, A.P., Rothberg, A., Hilboll, A., Kloeckner, A., Scopatz, A., Lee, A., Rokem, A., Woods, C.N., Fulton, C., Masson, C., Häggström, C., Fitzgerald, C., Nicholson, D.A., Hagen, D.R., Pasechnik, D.V., Olivetti, E., Martin, E., Wieser, E., Silva, F., Lenders, F., Wilhelm, F., Young, G., Price, G.A., Ingold, G.-L., Allen, G.E., Lee, G.R., Audren, H., Probst, I., Dietrich, J.P., Silterra, J., Webber, J.T., Slavič, J., Nothman, J., Buchner, J., Kulick, J., Schönberger, J.L., De Miranda Cardoso, J.V., Reimer, J., Harrington, J., Rodríguez, J.L.C., Nunez-Iglesias, J., Kuczynski, J., Tritz, K., Thoma, M., Newville, M., Kümmerer, M., Bolingbroke, M., Tartre, M., Pak, M., Smith, N.J., Nowaczyk, N., Shebanov, N., Pavlyk, O., Brodtkorb, P.A., Lee, P., McGibbon, R.T., Feldbauer, R., Lewis, S., Tygier, S., Sievert, S., Vigna, S., Peterson, S., More, S., Pudlik, T., Oshima, T., Pingel, T.J., Robitaille, T.P., Spura, T., Jones, T.R., Cera, T., Leslie, T., Zito, T., Krauss, T., Upadhyay, U., Halchenko, Y.O., Vázquez-Baeza, Y., 2020. SciPy 1.0: fundamental algorithms for scientific computing in Python. Nat. Methods 17, 261–272. https://doi.org/10.1038/s41592-019-0686-2

Wang, H., Lu, W., Wang, W., Liu, Q., Yamamoto, J., 2024. High-precision analysis of carbon isotopic composition for individual CO2 inclusions via Raman spectroscopy: Addressing issues arising from the laser-heating effects. Chem. Geol. 651, 122014. https://doi.org/10.1016/j.chemgeo.2024.122014

Wang, H.A.O., Cartier, L.E., Baumgartner, L.P., Bouvier, A.-S., Bégué, F., Chalain, J.-P., Krzemnicki, M.S., 2018. A Preliminary SIMS Study Using Carbon Isotopes to Separate Natural from Synthetic Diamonds. J. Gemmol. 36, 38–43. https://doi.org/10.15506/JoG.2018.36.1.38

Wang, W., Lu, W., 2023. High-precision analysis of carbon isotopic composition for individual CO2 inclusions via Raman spectroscopy to reveal the multiple-stages evolution of CO2- bearing fluids and melts. Geosci. Front. 14, 101528. https://doi.org/10.1016/j.gsf.2022.101528